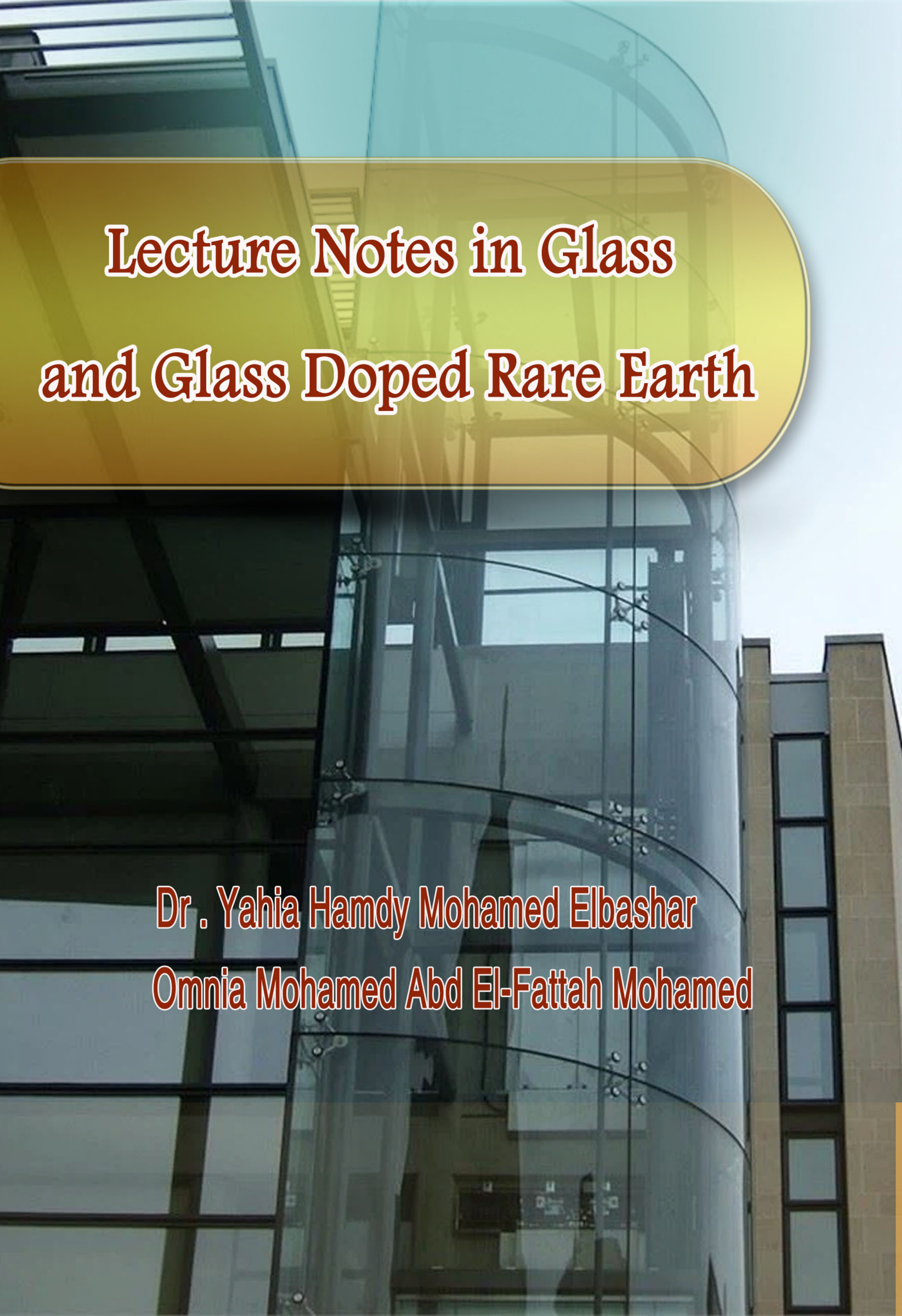

Lecture Notes in Glass and Glass Doped Rare Earth

Dr . Yahia Hamdy Mohamed Elbashar

Omnia Mohamed Abd El-Fattah Mohamed

Lecture Notes in Glass and Glass Doped Rare Earth

Prepared by:

Dr . Yahia Hamdy Mohamed Ibrahim Elbashar

د / يحيي حمدي محمد ابراهيم البشار

Omnia Mohamed Abd El-Fattah Mohamed Abd El-Fattah

أمنية محمد عبد الفتاح محمد عبد الفتاح

رقم الإيداع بدار الكتب والوثائق القومية

2022/15969

الترقيم الدولي: 978-977-94-2720-1

Table of contents

Introduction	3
Glass formation in oxides	3
Glass formation by cooling technique	4
Borate glass structure	6
Rare earth elements	9
Optical Properties of Rare-earth Ions	10
Applications of Rare-earth- Materials	12
Rare-earth in glass and fiber lasers	13
Laser Materials	14
Glass lasers	15
Literature survey	15
Appendix	24
References	29

1.1. Introduction

The word glass is usually used throughout most of history have been based on silica. It is possible to form an almost limitless number of inorganic glasses which do not contain silica, so silica is not a required component of a glass." Glasses are traditionally formed by cooling from a melt. However it can be prepared by different methods such as vapor deposition, by sol-gel processing of solutions, and by neutron irradiation of crystalline materials. Most traditional glasses are inorganic and non-metallic. We currently use a vast number of organic glasses. Metallic glasses are becoming more common with every passing year. Obviously the chemical nature of the material cannot be used to define a glass. All glasses exhibit two common characteristics. First, no glass has a long range, periodic atomic arrangement. And even more importantly, every glass exhibits time-dependent glass transformation behavior [1-20]. The glass has many applications like optical filters, nuclear shielding, laser protection, and even in water treatment and antibacterial effect [20-30]

This behavior occurs over a temperature range known as the glass transformation region. A glass can thus be defined as "an amorphous solid completely lacking in long range, periodic atomic structure, and exhibiting a region of glass transformation behavior." any material, inorganic, organic, or metallic, formed by any technique, which exhibits glass transformation behavior is a glass [1].

1.2. Glass formation in oxides

The most important commercial glasses are based on oxides; the ultimate condition for glass formation is that a substance form extended three-dimensional networks showing no long order. From this condition, it is derived four rules for oxide structure that allow one to choose those oxides that tend to form glasses as shown in Fig[1-1]. These rules were remarkably successful in predicting new glass- forming oxides as well as including such oxides known at the time of their formulation. The rules are the following [31]:

1. An oxygen atom is linked to not more than two glass-forming atoms.
2. The coordination number of the glass-forming atoms is small.
3. The oxygen polyhedra share corners with each other, not edges or faces.
4. The polyhedra are linked in a three-dimensional network.

Oxides A_2O or AO, where A is a metal atom, do not satisfy the rules. Oxides A_2O_3 satisfy rules 1, 3, and 4 if the oxygen atoms form triangles around each A atom, and AO_2 or A_2O_5 satisfy these rules if the oxygen atoms form tetrahedra around each A.

High coordination number is excluded by rule 2. This leads Zachariasen to concluded that the following oxides should be glass formers: B_2O_3, SiO_2, GeO_2, P_2O_5, As_2O_5, P_2O_3, As_2O_3, Sb_2O_3, V_2O_5, Sb_2O_5, Nb_2O_5, and Ta_2O_5. At the time of Zachariasen's research, only B_2O_3, SiO_2, GeO_2, P_2O_5, As_2O_5, and As_2O_3 had been made into glasses.

Zachariasen's rules are quite accurate in predicting glass formation, and it is interesting to question their relationship to the criteria for glass formation involving crystallization rates.

The requirement that the oxide form a three-dimensional network means that viscous flow is relatively difficult because it requires breaking-of primary chemical bonds, as shown in Fig[1-2]. In fact, Sun has shown that the glass-forming tendency of an oxide is directly related to the strength of the bonds between its oxygen and metal atoms [31]. Glass formers have bond strengths above about 80 kcal/mole, and modifying ions that are not part of the oxide network have oxygen-metal bond strengths below this value. Other correlations of glass-forming tendency of oxides have been made. Stanworth has suggested the following criteria [31]:

1. The cation valence must be three or greater.
2. The tendency to glass formation increases with decreasing cation size.
3. The electronegativity should be between about 1.5 and 2.1 on Pauling's scale.

Using these criteria Stanworth finds four groups of oxides: the strong glass formers, Si, Ge, As, P, and B; "intermediate" glass formers which form glasses only with "splat" cooling, Sb, V, W, Mo, and Te; other oxides that do not form glasses on rapid cooling, but do form them on oxidized surfaces of their metals or in binary combination with nonglass-forming oxides, Al, Ga, Ti, Ta, Nb, and Bi; and other oxides that do not form glasses. Poulain has suggested that glass formation in ionic systems occurs when a cation stabilizes the anion lattice, even if the field strength of the cation is not high. Thus in the zirconium fluoride glasses, zirconium ions stabilize the fluoride lattice [31].

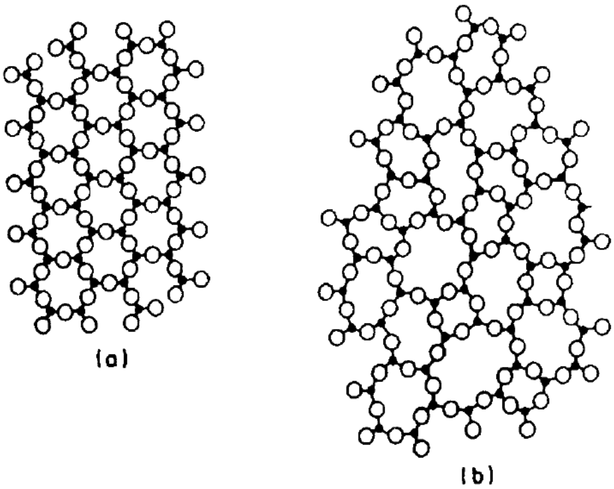

Fig [1-1] Structural representation of (a) A_2O_3 crystal and (b) A_2O_3 glass [32]

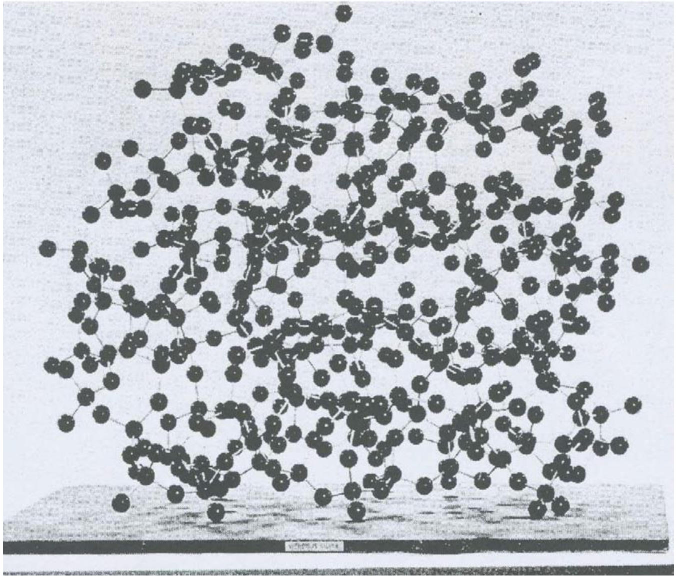

Fig [1-2] Continuous random network model simulating the structure of amorphous SiO_2 (After Bell and Dean, 1966) [32]

1.3. Glass formation by cooling technique

Figure [1.3] shows the dependence of specific volume (volume per unit mass) as a function of temperature. When the temperature of a liquid material is reduced, its volume decreases with decreasing temperature up to the freezing/melting point, T_m. At the freezing temperature, there is a remarkable sharp drop in the specific volume of the metal until it reaches the value characteristic of the solid crystalline. Further decrease in temperature below T_m results in a slow decrease of the volume, depending on its coefficient of thermal expansion.

Even though it was mentioned above that the specific volume decreases suddenly at the freezing temperature to transform into the crystal, a liquid normally undercools (or supercools, i.e., the liquid state can be maintained without crystallization occurring at temperatures well below the melting temperature) before crystallization can begin. This is because an activation energy barrier needs to be overcome before solid nuclei could form, and this activation barrier is smaller the larger the value of undercooling.

The degree of undercooling achieved depends on several factors, including the initial viscosity of the liquid, the rate of increase of viscosity with decreasing temperature, the interfacial energy between the melt and the crystal, the temperature dependence of the free energy difference between the undercooled melt and the crystal phases, the imposed cooling rate, and the efficiency of heterogeneous nucleating agents. Another way of increasing the amount of undercooling achieved is to increase the imposed cooling rate; the higher the cooling rate, the larger is the amount of undercooling. The situation in the case of a glass-forming liquid is different.

The volume decreases even in the under cooled region and its viscosity continues to increase. At some temperature, normally well below T_m, the viscosity becomes so high that the liquid gets “frozen in,” and this “frozen-in liquid” (it is like a solid for all practical purposes) is referred to as glass [33].

As defined above, the glass transition temperature, T_g, is the temperature at which the supercooled liquid becomes solid glass. To be more accurate, this should be called the thermal or calorimetric glass transition. It is also important to realize that this “transition” is not a true thermodynamic phase transition, but its origin is strictly kinetic, since the value of T_g depends on the cooling rate and, more generally, on the way the glass is prepared. The glassy state below T_g is often referred to as the “thermodynamic” state of a vitrified (glassy) substance. It is true that the properties of the glassy solid do not show any time dependence for not too long observation times and/or well below T_g. Therefore, it appears that the glassy solid is in a properly defined thermodynamic state. However, even in this case, time will always play a fundamental role in the formation and description of the glass, the fundamental reason simply being that it is not an equilibrium state. Glassy substances that look like a solid on experimental timescales of seconds or even years may look like a liquid on geological timescales. The non static nature of glass is seen the best near the glass transition [33].

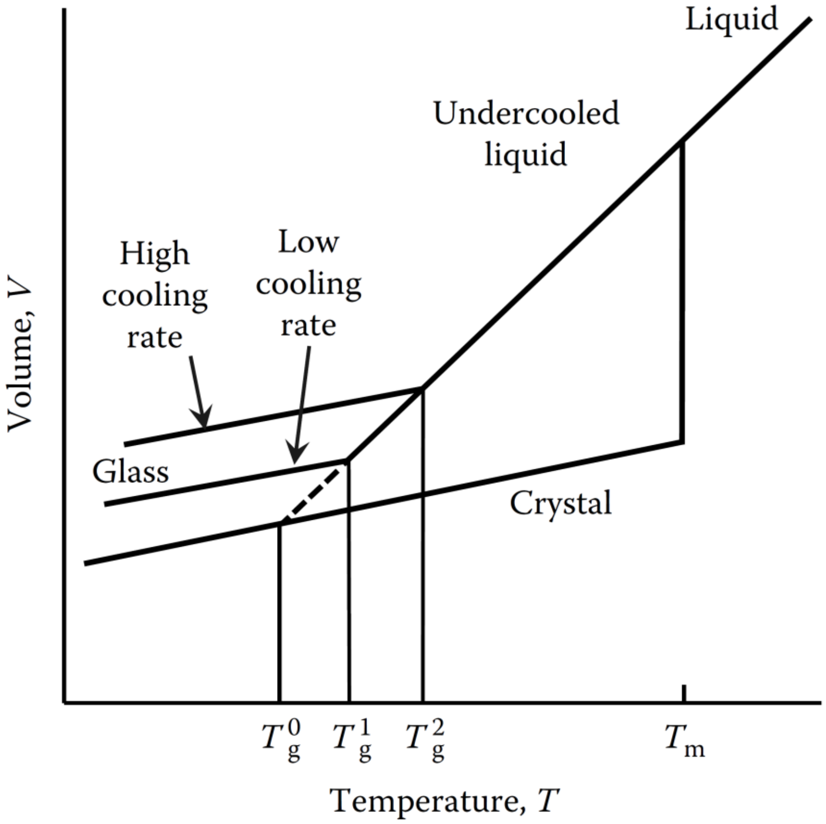

Figure [1-3] Variation of specific volume with temperature for a normal and a glass-forming material [33]

1.3.1. Borate glass structure

The coordination around each boron is only 3, so the basic structural unit of B_2O_3 glass is the $(BO_3)^{3-}$ triangle [34]. Figure [1-4] shows one possible B_2O_3 structure based on $(BO_3)^{3-}$ triangles. Other known structural units of B_2O_3 glass are shown in Figure [1-5] [35].

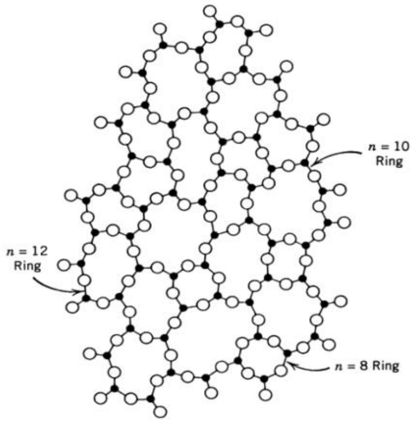

Figure [1-4] Sketch of the triangular structure of B_2O_3 glass. The black circles represent the 3-coordinated boron atoms, and the white circles represent the bridging oxygen atoms [35] (From Zachariasen [36]).

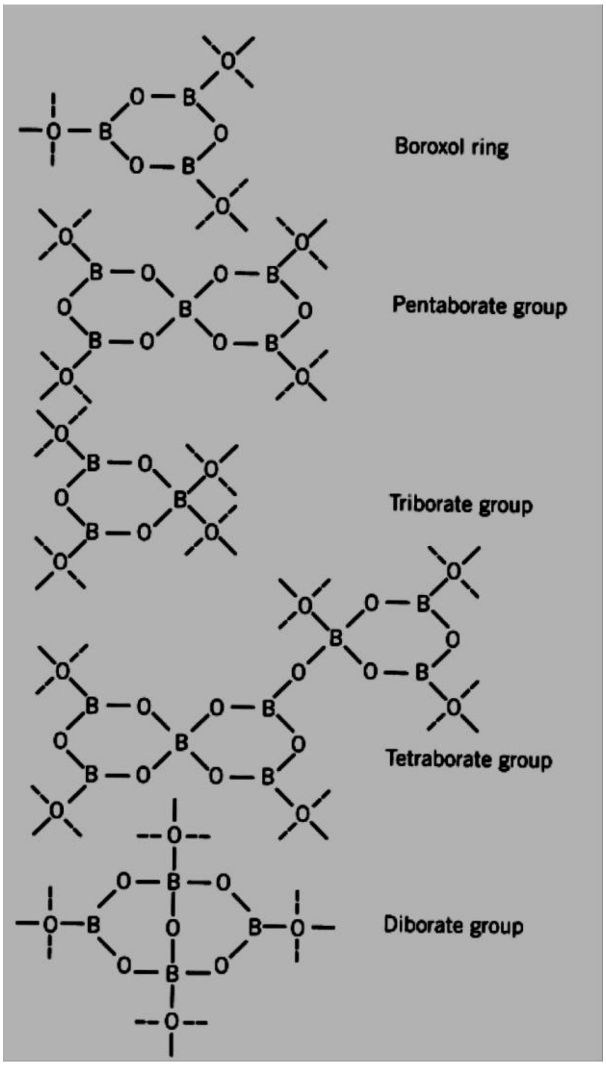

Figure [1-5] various structural elements of B_2O_3 glass[6] (From Vogel [37]).

The oxygen atoms in B_2O_3 form bridges between adjacent structural units. However, when an alkali impurity is added, it does not always create nonbridging oxygen. The alkali may instead convert boron from a 3- coordination state to a 4-coordination state, thereby making it tetrahedrally coordinated. These two possibilities are shown in Figures [1-6] and [1-7] [35].

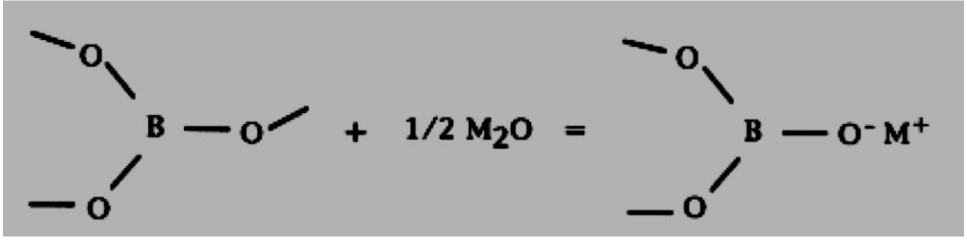

Figure [1-6] this sketch illustrates the formation of non bridging oxygen from the addition of an alkali oxide M_2O[35] (From Varshneya [38])

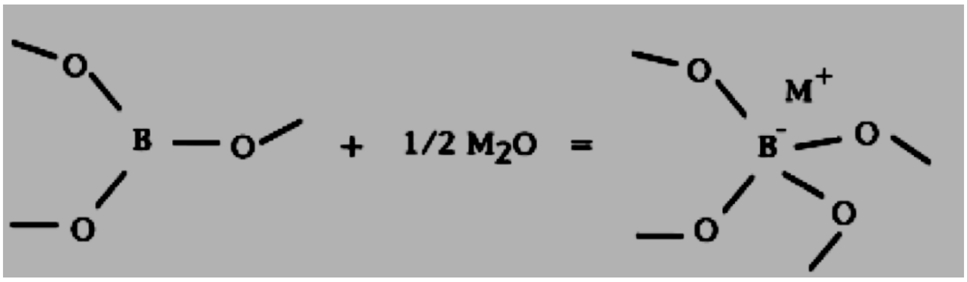

Figure [1-7] this sketch shows the conversion of boron from a 3-coordiation state to a 4-coordination state as a result of the addition of an alkali oxide M_2O[35] (From Varshneya [38]).

If an alkali impurity creates non-bridging oxygen, the connectivity of the B_2O_3 network decreases; however, if an alkali impurity causes boron to become tetrahedrally coordinated, the connectivity of the network increases. Because the connectivity of a B_2O_3 glass is greatly altered by either of these structural changes, the glass properties are also subject to change. Usually, the property changes resulting from the creation of non-bridging oxygen are directly opposite of the property changes caused by an increase in boron coordination [35].

This interesting structural phenomenon is known as the boron anomaly. Bray [39] experimentally determined the fraction of tetrahedrally coordinated boron as a function of alkali concentration. Figure [1-8] plots this data for several alkali borate glasses, with Na_2O and Li_2O being of particular interest to this experiment. The fraction of boron atoms in tetrahedral coordination increases until about 35-40 mole % alkali. The formation of non-bridging oxygen becomes apparent at greater alkali concentrations. Although there is no certain explanation for the boron anomaly, Varshneya[39] explains that the current proposed explanation regards “the anomaly as a manifestation of the various atomic groups in which boron may be found as a function of the various alkali additions.” Some of these various borate groups are shown in Figure [1-5]. The structural role of a network modifier is determined by the network-forming agent of the glass and the size and charge of the modifier. Since the two cations used in the experiment (Na^+ and Li^+) have the same charge, only cation size is a factor when comparing the properties of sodium borate and lithium borate glasses. This size difference must explain any differences in properties between these two types of glasses, given the same mole percent alkali [35].

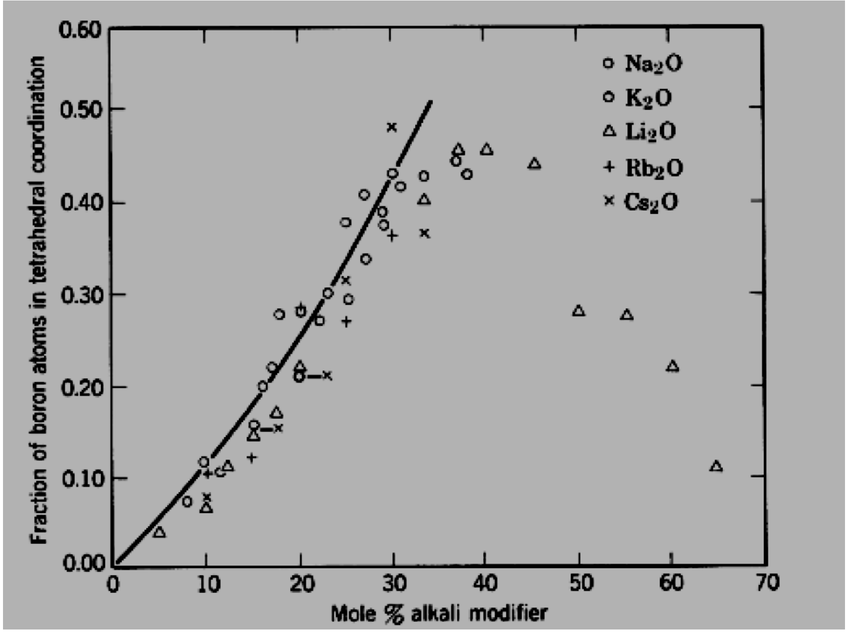

Figure [1-8] Graphical depiction of the boron anomaly [35] (From Bray [39]).

1.4. Rare earth elements

1.4.1. Introduction

The discovery of the rare earth begin with a rich stores of the rare earth minerals lay hidden for centuries in the Scandinavian peninsula until, one day in 1787, Lieutenant Carl Axel Arrhenius found, near the Ytterby feldspar quarry in Roslagen, an unusual black rock which he at first called ytterite, but which was later named gadolinite for the famous Finnish scientist Johan Gadolin who detected in it yttria, scandia, and all the rare earths of the yttria group [40].

The important of rare earth oxides begins from your personal items such as a portable compact disc player to a super computer or a huge atom-smashing accelerator, there are many rare earth materials having crucial roles in such systems. An automobile is a heap of rare earth materials. This is because rare earth ions exhibit some unique properties. Usefulness of rare earth materials for permanent magnets and luminescent materials for television and lighting systems goes without saying. Most of rare earth materials have been produced from rare earth oxides. Perovskite type rare earth mixed oxides are well known for high temperature super conductors, ferroelectric materials, or refining processes of rare earth metals needs their oxides as starting materials. Rare earth oxides are of importance for glass industry, for example, not only glass components but also surface polishing [41], fluorescent lamps, solid-state lasers, to optical amplifiers in fiber optics, rare earth (RE) elements, or lanthanides, have been widely used to activate luminescent and photonic materials [42]. The complete group of rare earth metals consists of the three elements scandium Sc, yttrium Y and lanthanum La and the fourteen lanthanides cerium to lutetium. The total number of REMs is thus 17. They are, for practical reasons, divided into two subgroups, the cerium group with the lighter elements and the yttrium group with the heavier ones (Table 1.1) [43].

Table 1.1 Two groups of rare earth metals [43]

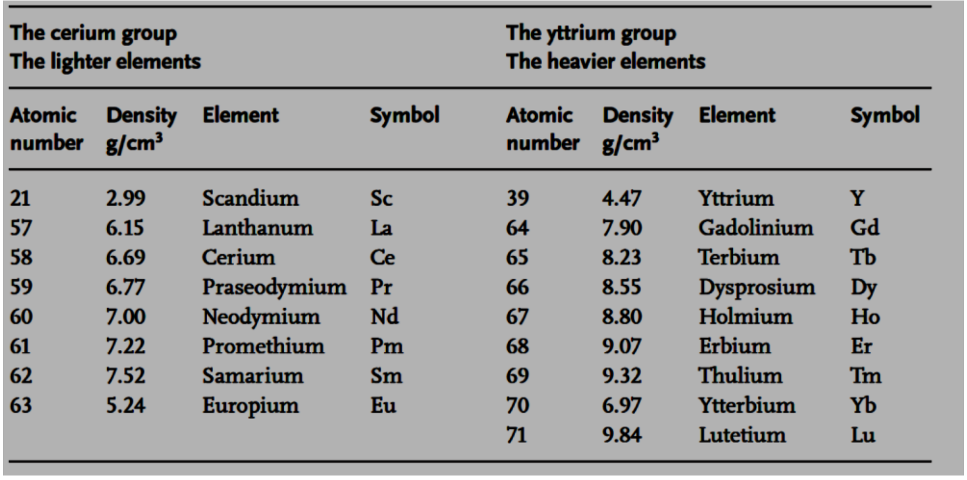

The cerium group The lighter elements				The yttrium group The heavier elements			
Atomic number	Density g/cm³	Element	Symbol	Atomic number	Density g/cm³	Element	Symbol
21	2.99	Scandium	Sc	39	4.47	Yttrium	Y
57	6.15	Lanthanum	La	64	7.90	Gadolinium	Gd
58	6.69	Cerium	Ce	65	8.23	Terbium	Tb
59	6.77	Praseodymium	Pr	66	8.55	Dysprosium	Dy
60	7.00	Neodymium	Nd	67	8.80	Holmium	Ho
61	7.22	Promethium	Pm	68	9.07	Erbium	Er
62	7.52	Samarium	Sm	69	9.32	Thulium	Tm
63	5.24	Europium	Eu	70	6.97	Ytterbium	Yb
				71	9.84	Lutetium	Lu

The use of rare earth increases every year, By 1975 the consumption was more than 20 x 10^3 metric tons and the main uses were in metallurgy (~45%), catalysts and chemicals (~36%), glasses and ceramics (~17%), and electronics (~2%) (Cannon, 1976). The increase and changes in emphasis were the direct result of much research on the nature and possible applications of those elements [44].

1.4.2 Optical Properties of Rare-earth Ions

A range of optical processes are relevant to rare-earth spectroscopy, the most obvious being one-photon transitions within the $4f^N$ configuration. However, other processes are also of interest. These include two-photon transitions (two-photon absorption, Raman scattering and second harmonic generation), circular dichroism, and transitions outside of the $4f^N$ configuration. In the latter case there is the possibility of exciting a 4f electron into a 5d orbital, or exciting a ligand electron into a 4f orbital, a charge-transfer transition. Detailed modeling of transition probabilities within the $4f^N$ configuration dates back to Judd (1962) and Ofelt (1962). The total intensities between J multiples, However, transitions between crystal-field levels were examined by Axe (1963), who also carried out the first calculations for two-photon processes (Axe, 1964). Electric-dipole transitions within the $4f^N$ configuration are forbidden in the absence of an odd-parity interaction with the crystal. The considered only the mixing of atomic configurations by the crystal field, summarized by Peacock (1975), demonstrated that excitations involving ligand states (dynamic polarization and charge transfer) were also important. Significant progress in both understanding the underlying mechanisms and phenomenological modeling of the transitions has been made over the last two decades, for both one-photon (Gorller-Wakand and Binnemans, 1998; Smentek, 1998; Reid, 2000) and two photon transitions (Downer, 1989; Nguyen, 1997) [42].
The widely circulated Dieke chart of energy level structure in the RE series was first created for trivalent ions in $LaCl_3$ based on the analyses of limited spectra (Dieke, 1968) [42] as shown in Figure [1-9] [45]. The most significant feature of the RE ions is the partial filling of the 4f electron shell. The closed electron shells correspond to a xenon core $1s^2 2s^2 2p^6 3s^2 3p^6 3d^{10} 4s^2 4p^6 4d^{10} 5s^2 5p^6$, which is the ground spectroscopic state of La^{3+} or Ce^{4+}. In the following ions electrons are added successively into the 4f shell, until it is full with 14 electrons at Yb^{2+} and Lu^{3+}. The number of LS terms increases when increasing the number of 4f electrons from 1 to 7 and decreases when increasing the number of 4f electrons from 7 to 14. In the intermediate coupling approximation, all LS terms are split by spin–orbit interaction into JJ manifolds, the number of which follows the same trend for the LS terms above. Each manifold can be split further if an ion is embedded into a crystal or a glass with the number of resulting states depending on the symmetry of the environment (residual

double degeneracy of all energy levels which can be removed by magnetic field only remains for the Kramers ions, i.e. Ce^{3+}, Nd^{3+}, Sm^{3+}, Gd^{3+}, Dy^{3+}, Er^{3+}, and Yb^{3+}, having odd numbers of 4f electrons). The use of the UV or VUV excitation can promote one of 4f electrons of a RE ion into 5d orbital leading to the change of the electron configuration from $4f^n$ to $4f^{n-1}5d$. Table 1.2 gives the basic information about the ground and first excited electron configurations of the RE^{3+} ions. Large numbers of states in the ground and first excited configurations (especially for the ions in the middle part of the RE series) open an opportunity for getting an emission in a wide spectral domain, as well as combining different ions to get an effective energy transfer from one to another (provided the resonance condition between the energy levels of interest is fulfilled). In general, since the electronic transitions within the ground configuration are parity forbidden and become allowed only due to the admixture of states of opposite parity, the corresponding absorption and emission lines are very narrow and they are slightly dependent on the environment (because of the screening effect from the outer shells). On the contrary, the absorption spectra ascribing to the interconfigurational $4f^n \rightarrow 4f^{n-1}5d$ transitions are associated with very broad bands and significantly affected by the electron-vibronic interaction [45].

Table 1.2 Main characteristics of the ground and first excited electron configurations of trivalent RE[45]

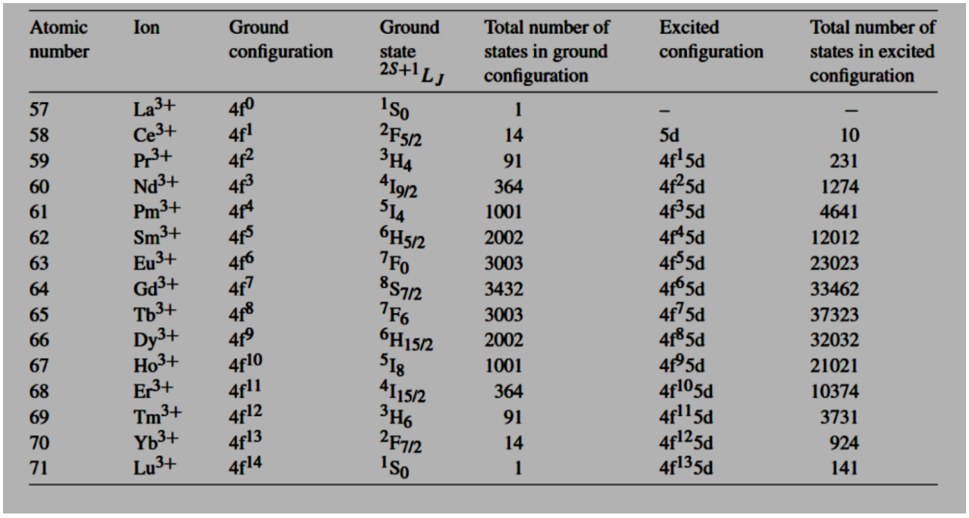

Atomic number	Ion	Ground configuration	Ground state $^{2S+1}L_J$	Total number of states in ground configuration	Excited configuration	Total number of states in excited configuration
57	La^{3+}	$4f^0$	$^1S_0$	1	–	–
58	Ce^{3+}	$4f^1$	$^2F_{5/2}$	14	5d	10
59	Pr^{3+}	$4f^2$	$^3H_4$	91	$4f^15d$	231
60	Nd^{3+}	$4f^3$	$^4I_{9/2}$	364	$4f^25d$	1274
61	Pm^{3+}	$4f^4$	$^5I_4$	1001	$4f^35d$	4641
62	Sm^{3+}	$4f^5$	$^6H_{5/2}$	2002	$4f^45d$	12012
63	Eu^{3+}	$4f^6$	$^7F_0$	3003	$4f^55d$	23023
64	Gd^{3+}	$4f^7$	$^8S_{7/2}$	3432	$4f^65d$	33462
65	Tb^{3+}	$4f^8$	$^7F_6$	3003	$4f^75d$	37323
66	Dy^{3+}	$4f^9$	$^6H_{15/2}$	2002	$4f^85d$	32032
67	Ho^{3+}	$4f^{10}$	$^5I_8$	1001	$4f^95d$	21021
68	Er^{3+}	$4f^{11}$	$^4I_{15/2}$	364	$4f^{10}5d$	10374
69	Tm^{3+}	$4f^{12}$	$^3H_6$	91	$4f^{11}5d$	3731
70	Yb^{3+}	$4f^{13}$	$^2F_{7/2}$	14	$4f^{12}5d$	924
71	Lu^{3+}	$4f^{14}$	$^1S_0$	1	$4f^{13}5d$	141

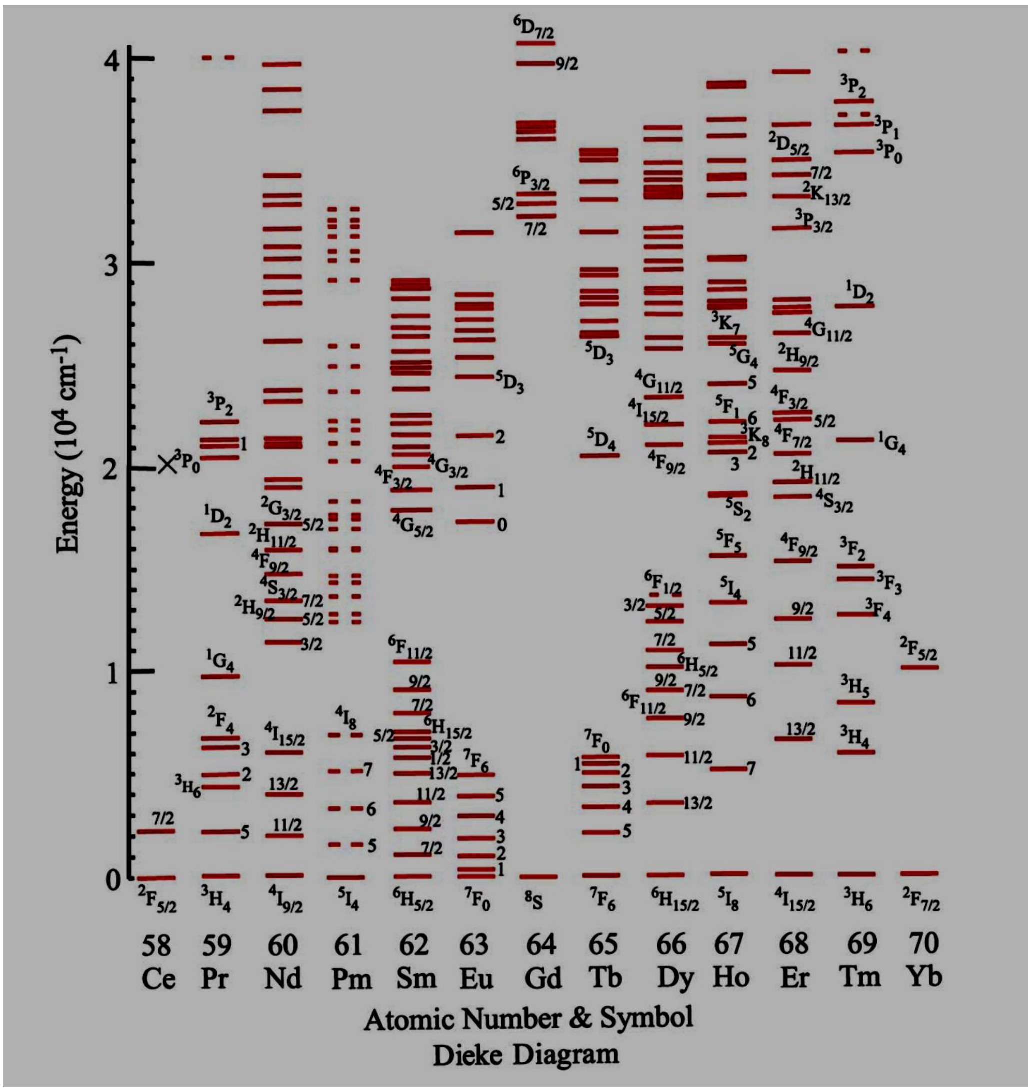

Figure [1-9]Dieke diagram (energy levels of free RE^{3+} ions up to 42000 cm^{-1}) [45].

1.4.3. Applications of Rare-earth- Materials

Rare-earth ions play an important role in modern technology as the active constituents of many optical materials. There are a vast number of applications for these rare-earth activated materials, and much of today's cutting-edge optical technology and emerging innovations are enabled by their unique properties, such as optical properties of new materials and effective search for new crystals and activator ions for various applications in quantum electronics [45]. Many applications of lanthanide materials make use of the 4f^{n-1}5d excited configuration. These applications include scintillator materials, VUV lasers, and phosphors for fluorescent lighting and plasma displays (Blasse and Grabmaier, 1994; Feldmann et al., 2003). An understanding of these states is crucial to the development of advanced materials [45]. The spectroscopic properties and luminescence dynamics of lanthanide ions in nanomaterials, Promising applications such as nanophosphors for high resolution display devices [45]. The lanthanide luminescence can be efficiently sensitized by exciton recombination in the semiconductor nanocrystals. Potential applications of luminescent lanthanide-doped semiconductor nanocrystals include single color or white light emitting devices (LEDs) [45].

1.4.4. Rare-earth in glass and fiber lasers

Rare earths have important characteristics that distinguish them from other optically active ions: they emit and absorb over narrow wavelength ranges, the wavelengths of the emission and absorption transitions are relatively insensitive to host material, the intensities of these transitions are weak, the lifetimes of metastable states are long, and the quantum efficiencies tend to be high, except in aqueous solutions. These properties all result from the nature of the states involved in these processes and lead to excellent performance of rare earth ions in many optical applications. Devices that provide gain, such as lasers and amplifiers, must have low scattering losses, and one is restricted to using single-crystal or glass hosts. Whereas in many applications crystalline materials are preferred for reasons that include higher peak cross sections or better thermal conductivities, the versatility of glasses and the broader emission and absorption spectra they provide have led to the use of rare earth doped glasses in many applications. Nowhere is this truer than in the area of optical fiber devices. Table 1.3 lists the wavelengths, transitions, and features of fiber lasers and amplifiers that had been reported as of 1991. Oxide and fluoride hosts are distinguished in the table, because the latter provide more metastable states and greater transparency at wavelengths beyond 2000 nm. The high intensities and long interaction lengths made possible by fiber waveguides make these devices vastly superior to their bulk glass counterparts in most applications [46].

Table1.3 Glass Fiber Lasers and Amplifiers [46]

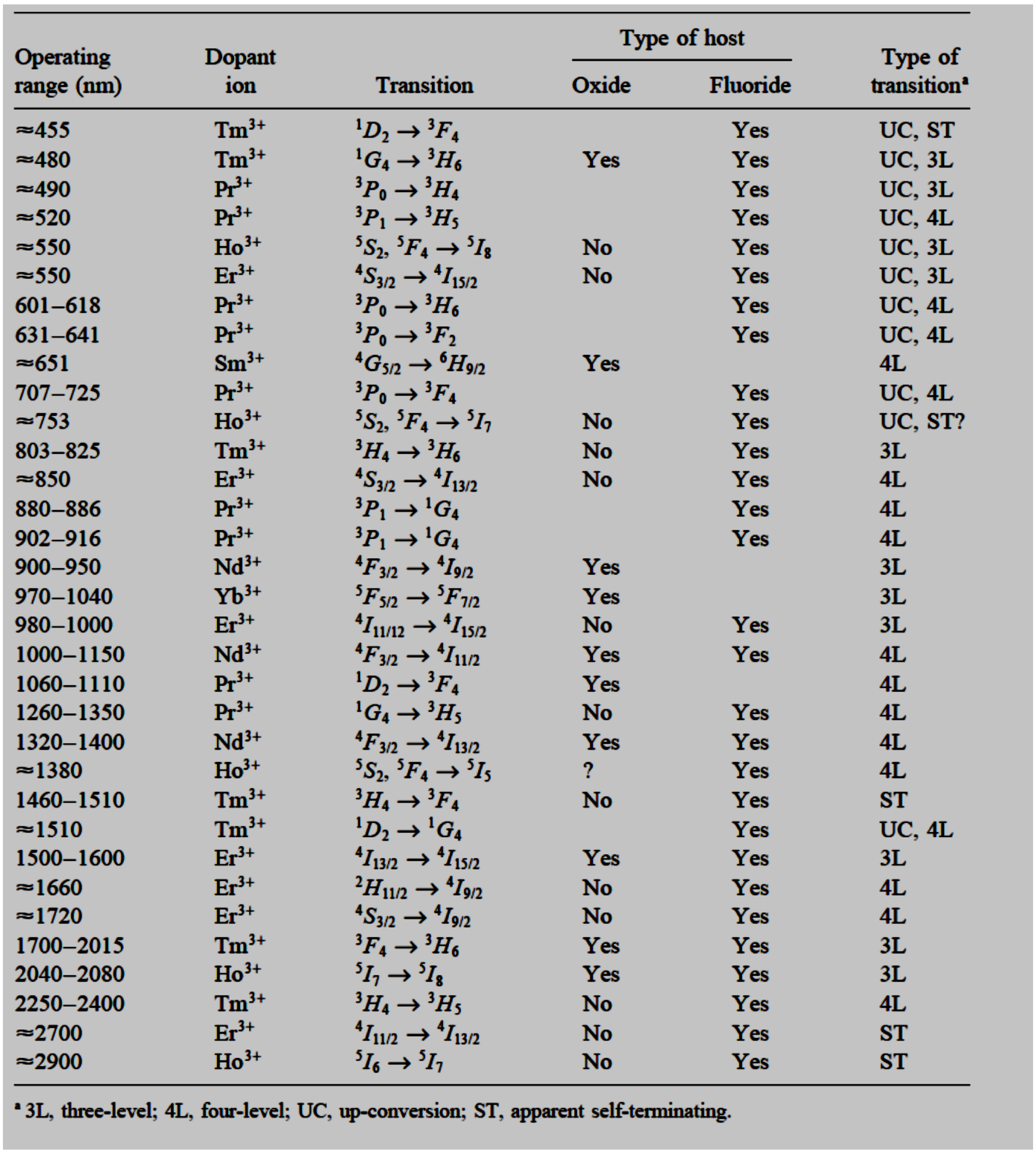

Operating range (nm)	Dopant ion	Transition	Type of host		Type of transition[a]
			Oxide	Fluoride	
≈455	Tm^{3+}	$^1D_2 \rightarrow {}^3F_4$		Yes	UC, ST
≈480	Tm^{3+}	$^1G_4 \rightarrow {}^3H_6$	Yes	Yes	UC, 3L
≈490	Pr^{3+}	$^3P_0 \rightarrow {}^3H_4$		Yes	UC, 3L
≈520	Pr^{3+}	$^3P_1 \rightarrow {}^3H_5$		Yes	UC, 4L
≈550	Ho^{3+}	$^5S_2, {}^5F_4 \rightarrow {}^5I_8$	No	Yes	UC, 3L
≈550	Er^{3+}	$^4S_{3/2} \rightarrow {}^4I_{15/2}$	No	Yes	UC, 3L
601–618	Pr^{3+}	$^3P_0 \rightarrow {}^3H_6$		Yes	UC, 4L
631–641	Pr^{3+}	$^3P_0 \rightarrow {}^3F_2$		Yes	UC, 4L
≈651	Sm^{3+}	$^4G_{5/2} \rightarrow {}^6H_{9/2}$	Yes		4L
707–725	Pr^{3+}	$^3P_0 \rightarrow {}^3F_4$		Yes	UC, 4L
≈753	Ho^{3+}	$^5S_2, {}^5F_4 \rightarrow {}^5I_7$	No	Yes	UC, ST?
803–825	Tm^{3+}	$^3H_4 \rightarrow {}^3H_6$	No	Yes	3L
≈850	Er^{3+}	$^4S_{3/2} \rightarrow {}^4I_{13/2}$	No	Yes	4L
880–886	Pr^{3+}	$^3P_1 \rightarrow {}^1G_4$		Yes	4L
902–916	Pr^{3+}	$^3P_1 \rightarrow {}^1G_4$		Yes	4L
900–950	Nd^{3+}	$^4F_{3/2} \rightarrow {}^4I_{9/2}$	Yes		3L
970–1040	Yb^{3+}	$^5F_{5/2} \rightarrow {}^5F_{7/2}$	Yes		3L
980–1000	Er^{3+}	$^4I_{11/12} \rightarrow {}^4I_{15/2}$	No	Yes	3L
1000–1150	Nd^{3+}	$^4F_{3/2} \rightarrow {}^4I_{11/2}$	Yes	Yes	4L
1060–1110	Pr^{3+}	$^1D_2 \rightarrow {}^3F_4$	Yes		4L
1260–1350	Pr^{3+}	$^1G_4 \rightarrow {}^3H_5$	No	Yes	4L
1320–1400	Nd^{3+}	$^4F_{3/2} \rightarrow {}^4I_{13/2}$	Yes	Yes	4L
≈1380	Ho^{3+}	$^5S_2, {}^5F_4 \rightarrow {}^5I_5$	?	Yes	4L
1460–1510	Tm^{3+}	$^3H_4 \rightarrow {}^3F_4$	No	Yes	ST
≈1510	Tm^{3+}	$^1D_2 \rightarrow {}^1G_4$		Yes	UC, 4L
1500–1600	Er^{3+}	$^4I_{13/2} \rightarrow {}^4I_{15/2}$	Yes	Yes	3L
≈1660	Er^{3+}	$^2H_{11/2} \rightarrow {}^4I_{9/2}$	No	Yes	4L
≈1720	Er^{3+}	$^4S_{3/2} \rightarrow {}^4I_{9/2}$	No	Yes	4L
1700–2015	Tm^{3+}	$^3F_4 \rightarrow {}^3H_6$	Yes	Yes	3L
2040–2080	Ho^{3+}	$^5I_7 \rightarrow {}^5I_8$	Yes	Yes	3L
2250–2400	Tm^{3+}	$^3H_4 \rightarrow {}^3H_5$	No	Yes	4L
≈2700	Er^{3+}	$^4I_{11/2} \rightarrow {}^4I_{13/2}$	No	Yes	ST
≈2900	Ho^{3+}	$^5I_6 \rightarrow {}^5I_7$	No	Yes	ST

[a] 3L, three-level; 4L, four-level; UC, up-conversion; ST, apparent self-terminating.

The borate glass for laser medium offer a uniform picture in their fluorescent properties, and all alkali borate glasses with all three common alkalis (Li, Na, and K) have nearly identical Nd^{3+} spectra over the whole glass-forming region. The fluorescence life time is shorter (about 150 µs) but the absorption intensity is a few times stronger for a comparable weight percentage of Nd because of the smaller atomic weight of boron and consequent changes in the phonon spectrum [47].

1.5. Laser Materials

The laser can be categorized from the materials into [48]:

Solid state lasers
Crystalline Paramagnetic Ion Lasers
Glass Lasers
Solid State Dye Lasers
Color Center Lasers
Semiconductor Lasers
Polymer Lasers
Liquid lasers
Organic Dye Lasers

Rare Earth Liquid Lasers
Gas lasers
Neutral Atom
Ionized
Molecular

Some lasers are not familiar to many readers or not commercially used as[48]:
Free electron lasers
Nuclear pumped lasers
Natural lasers
Inversionless Lasers

1.5.1. Glass lasers

The laser transition can be changed due to the glass host, and the changing cannot be expected as usual transition, not only that but also there are some heavy metals can share the lanthanides in the work as an active ion laser and they called sensitizing ions [48, 49]. The lasing transitions for these ions and approximate wavelengths are given in Table1.4. Some ions in glasses exhibiting gain are given in Table1.5. [48], the arrangement of glass lasers in order of increasing wavelength as shown in table1.6 [48].

1.6. Literature survey

D.S. Funk et al. [50]. He observed a lasing in the ultraviolet region in neodymium-doped fluorozirconate glass (ZBLAN) fibres at room temperature. The cavity output coupling of < 0.1%, 74µW of power was obtained at 381nm (4D3/2 → 4I11/2 transition of Nd3+) when a 45cm long fiber was pumped with 275mW at a wavelength of nominally 590nm.
D.S. Funk et al. [51]. He found a lasing as a Continuous oscillation on the 2P3/2 → 4I11/2 transition of Nd3+ in a fluorozirconate glass (ZBLAN) fiber at room temperature. The pumped at ,590 nm, a Nd:ZBLAN fiber 39 cm in length lases in the violet at 412 nm and produces ~0.5 mW of power for 320 mW of pump power and a cavity output coupling of 0.4%. The breadth of the laser's excitation spectrum is ~12 nm (581–593 nm).
M. Nikl et al. [52]. He shows the Photoluminescence spectra and its decay kinetics at room temperature for ZnO-containing mixed-oxide glasses of various compositions. He observed a dominant broad emission band peaking round 390 nm in most of the glasses. This emission is ascribed to the ZnO-aggregates originating both in their volume and at the interface with the glass host.
J.H. Campbell et al. [53]. He studied the composition and properties of neodymium-doped (Nd-doped) phosphate glasses that used for simultaneous high energy (10^3±10^6 J) and high-peak-power (10^{12}±10^{15} W) which used in laser of fusion energy research, he reviewed. He shows the most common base glasses are that meta-phosphates (O/P ~3) with the approximate composition: $60P_2O_5$-$10Al_2O_3$-$30M_2O$/MO; K/Ba or K/Mg are typical modifiers. He found the spectroscopy of Nd^{3+} in these glasses is well understood and laser properties can be accurately determined from measured spectroscopic properties. The major mechanisms of Nd^{3+} that he show is the non-radiative relaxation, and the empirical expressions that that predict of these effects in phosphate glasses.
Xiushan Zhu et al. [54]. He reviewed the most stable heavy metal fluoride glass and that is excellent host for rare-earth ions that used for laser applications. He reviewed also the

historical progress and the properties of fluoride glasses and the fabrication of ZBLAN fibers, and the advances of infrared, upconversion, and supercontinuum, constraints on the power scaling of ZBLAN fiber lasers. He shows the promise of generating high power emissions covering from ultraviolet to mid-infrared considering , which are recent advances in newly-designed optical fibers, beam-shaped high power pump diodes, beam combining techniques, and heat-dissipating technology.

S.P. Tandon et al. [55]. He studied the Neodymium-doped borate and phosphate glass as a lasing materials, he have been prepared the specimens by melt quenching technique. He observed the absorption spectra in the region 400 -900 nm. From observed absorption spectra he calculated the Judd Ofelt (JO),Ω_t parameters ($t = 2$, 4 and 6). He calculated the laser parameters, viz., spontaneous emission probability (A), fluorescence branching ratio (β) and stimulated emission cross-section (σ), and The effects of composition and concentration of the doping.

M. Weber et al. [56]. He measured the optical absorption and emission spectra and fluorescence lifetimes for Nd3+ in tellurite glasses containing various alkali and higher valence state cations and in a series of new phosphotellurite glasses, and he determined the Judd, Ofelt intensity parameters were and calculate radiative lifetimes and stimulated emission cross sections for 4F3/2→4I11/2 and 4F3/2→4I13/2 transitions. He determined also the cross sections for several oxide glasses.

John D. Myers et al. [57]. He observed a simultaneous dual- and multiple-wavelength operation and laser performance of 1.3 μm transition in various Nd3+-doped glasses, the simultaneous operation of both the 4F3/2 - 4I13/2 and the 4F3/2 - 4I11/2 transitions of Nd3+ in phosphate, silicate, and germanate glasses. Laser output from these two transitions demonstrates good temporal and spatial overlap. A slope efficiency of 1.1% was achieved in Q-100 phosphate laser glass. The resonator loss analysis indicates that there is no significant excited state absorption at 1.355 micrometer for phosphate glasses.

H. Jiang et al. [58]. He dominant issues known to limit pump power conversion efficiency include solarization from the Xe lamp's UV spectral component, and amplified spontaneous emission (ASE) from the Nd3+, and the spectral mismatch in Xe output power with the strongest absorption bands of the Nd3+. He observed the synergistic interactions in a phosphate glass doped with Ce3+ to prevent solarization, Sm3+ to inhibit ASE, and Eu3+ to radiatively sensitize the Nd3+ absorbing the portion of the Xe emission spectrum previously unused. This triply doped system is shown to enhance the output power from the Nd3+ laser rod by 50 % over undoped analogs.

A. E. Siegman et al. [59]. He reported a laser oscillation in a single transverse mode with very large mode area in optical fibers having heavily Nd-doped 100 μm diameter cores with refractive index significantly lower in the core than in the surrounding cladding. Since fibers of this type cannot support conventional index-guided modes, their results appear to confirm a recent analysis which predicts gain-guided single-mode propagation in index antiguided fibers, provided the gain coefficient in the core exceeds a threshold value. Fibers of this type may be of significant interest for amplifiers and oscillators having large power outputs and/or small nonlinear pulse distortion.

R. Jacobs et al. [60]. He studied the spectral intensities using the Judd-Ofelt (J-O) theory for crystal-field-induced electric dipole transitions demonstrate that Nd-doped glasses can be tailored for specific laser applications by proper selection of the glass constituents. He shows variations with glass composition are reported for the following properties: induced emission cross section, peak fluorescence wavelength, effective fluorescence bandwidth, radiative lifetime, transition probabilities, and fluorescence branching ratios. Both glass network formers and network-modifier ions were changed. The cross section for the Nd3+, 4F3/2 – 4I11/2 laser transition was varied by more than a factor of 4 by changing the glass host.

C. Jacinto et al. [61]. He studied the thermal lens technique experimentally to determine the influence of the energy transfer upconversion (ETU) processes on fluorescence quantum efficiency (η) in Nd3+-doped materials. The samples with high Nd3+ concentration present a considerable reduction in η with the increasing excitation power due to the efficient ETU processes. it was verified that the critical inversion density is not concentration independent, as previously stated, but it decreases with the Nd concentration. His results point out the approach based on TL technique as a valuable alternative because of its sensitivity allowing the measurements to be performed in a pump power regime that avoids damages in the investigated material.

C. Jacinto et al. [62]. He present a new method based on thermal lens (TL) technique to determine the fluorescence quantum efficiency, η, and thermo-optical coefficients of fluorescent materials. He obtained the TL signal with the experimental lifetimes of a set of samples with different luminescent ion concentrations. The method was applied in Nd3+-doped materials (Q-98 Phosphate, fluorozirconate, and fluoroindate).

S. L. Oliveira et al. [63]. He investigated the quantum efficiency values using a new Thermal Lens approach based on the 4F3/2 lifetimes value in Nd-doped phosphate laser glass, Q-98 glass.

John D. Myers et al. [64]. He developed a new end-pump double clad fiber laser designs fabricated from high performance phosphate laser glass compositions. One DC (Double Clad) LMA fiber is doped with erbium/ytterbium for 1.54um laser emission. Another DC LMA fiber is doped with ytterbium for 1.03um laser emission. A third DC multiple core "supermode" fiber is doped with neodymium for 1.053um laser emission. The erbium/ytterbium & ytterbium only doped fibers are end-pumped at 940/975nm with 40-Watt fiber coupled laser diodes. The neodymium-doped fiber is end-pumped with an 808nm 40-Watt fiber coupled laser diodes. Design and performance data for new side-pumped, highly doped phosphate DC LMA fiber laser architectures.

Ruikun Wu et al. [65]. He designed A number of double clad (DC) or cladding pumped neodymium doped phosphate glass fibers. One fiber contains a 50-micron diameter core doped with 9 wt.% Nd2O3 and a 0.18 NA. The inner cladding is made from undoped glass with 1.5mm x 1.5mm cross-section and exhibits a 0.62 NA with a low index silicone polymer outer cladding. Both annealed and un-annealed fibers were tested. The measured absorption for a 53 cm long un-annealed fiber was 73%, or 5.7 db. An 808nm fiber coupled diode array was used to end pump the neodymium fiber. Fiber laser action was observed in both pulsed and CW operation at 1.054um. Approximately 4.3 mj of pump energy was required to reach lasing threshold without resonator mirrors, (Fresnel reflection resonator only). A maximum of 2.1 Watts CW output power was obtained with 8.3 Watts absorbed pumping power using a 50% R output coupler. 34% slope efficiency was obtained with absorbed pump power.

S. Mohan et al. [66]. He studied the effect of increasing the rare earth ion concentration on the physical and spectroscopic properties of Nd3+ doped sodium-lead-borate glasses for the compositions (10-x) Na2O–30PbO–60B2O3– xNd2O3, where x = 1.00, 1.25, 1.50, 1.75 and 2.00 mol %. Optical band gaps, cut-off wavelengths and various spectroscopic parameters (E1, E2, E3, F2, F4, F6 and x4 f) have been determined from the room temperature absorption spectra. Judd-Ofelt theory has been employed to determine the intensity parameters W2, W4 and W6 which in turn are used to evaluate radiative transition probability (A), branching ratio (b) and radiative lifetime (tr) for the fluorescent level 4F3/2. The W2 parameter and hence the non-symmetric component of electric field acting on Nd3+ ion is found to be highest for glass with 1.75 mol% of Nd2O3. He shows that a poor resolution of hypersensitive transition, the covalency of the Nd-O bond has been characterized by the relative intensity of 4I9/2 -> 4F7/2, 4S3/2. The highest covalency has been predicted for glass with 2 mol% Nd2O3. The radiative properties are found to improve with an increase in concentration of Nd2O3.

S. Jiang et al. [67]. He enhanced of the thermal loading capability for both Er3+ and Nd3+ doped inherently strong glasses by an ion-exchange chemical strengthening process. A free running laser with an average output power of 6.5 W and a Q-switched single mode laser with energy of 5 mJ at a repetition rate of 15 Hz have been demonstrated at the 1.54 mm eye-safe wavelength with strengthened QX/Er glass. An average output power of 110 W at 1.05mm has been obtained employing a strengthened QX/Nd glass rod.

Wojciech A. Pisarski et al. [68]. He studied the influence of rare earth ions on structural behavior in lead borate glasses using infrared spectroscopy. The structural changes have been analyzed with increasing rare earth concentration. Partial BO34 ←→BO4 conversion as a function of rare earth concentration is observed only for the smaller heavier lanthanides, whereas for the larger lighter lanthanides the concentration effect.

J. Furthner et al. [69]. He studied the emission spectra and cross-section spectra of neodymium laser glasses by amplified spontaneous emission spectra and light amplification spectra of some Nd3 +:glass rods (silicate glass Schott LG680, phosphate glasses Schott LG760 and Hoya LHG5) are measured by pulsed flashlamp excitation. The spontaneous emission distribution, the stimulated emission cross-section spectra and the excited state absorption cross-section spectra are extracted. Excited state absorption prevents laser action around 1320 nm for the 4F3/2 - 4l13/2 transition of Nd3 + in the investigated glasses.

M.Zahir et al. [70]. He studied the structural interaction of the Pb2+, Eu3+ and Nd3+ doped in sodium borate glasses over the compositional range 10-35 mol.% Na2O. he found that a two possible situations depending on Na2O content is lower or higher than about 25 mol.%. In the first composition range the simultaneous increase of optical basicity and of modifier ion site asymmetry implies rather a 2D-character of the network former. The properties of the glasses with high Na20 content involve more 3D-character for the former sublattice.

A.E. Burns et al. [71]. He studied the structure of binary neodymium borate glasses by infrared spectroscopy. A new series of binary rare earth oxide borate glasses were synthesized, with general formula xNd2O3 + (1 - x) B2O3, where x varies up to 35 mol%. The results show that the neodymium acts as a modifier, similar to an alkali metal. As x is increased, the borate glass network is shown to change from a three-coordinated to four-coordinated boron system. The results are further investigated by analyzing the spectra in terms of the location of the bands to show how the borate groups change upon neodymium addition.

L. Del Longo et al. [72]. He studied the optical spectroscopy of zinc borate glass activated by Pr3+ ions with chemical compostion of the zinc borate glass as 4ZnO.3B2O3, with different concentrations of Pr3+. The investigated for luminescence spectroscopies of energy levels and optical transitions of Pr3+ in zinc borate glass are assigned at low Pr3+ concentration the luminescence is dominated by emission from the 1D2 state which is populated by fast multiphonon relaxation from the 3P0 state. At Pr3+ concentrations higher than 2% mol energy transfer processes become efficient in the relaxation of the 3P0 state. Cross relaxation dominates the 1D2 depopulation in the full range of Pr3+ concentrations. Self-absorption of the 3P0 --> 3H4 luminescence was observed for glassed doped with 4% and 8% mol Pr3+.

Selcuk Akturk et al. [73]. He designed a designed and demonstrated a very simple and compact ultrashort-pulse compressor using a single glass prism and a corner-cube. The design is significantly easier to align. Angle-tuning the prism wavelength-tunes, and translating the corner cube varies the group-delay dispersion over a wide range. When tuned, the device automatically maintains zero angular dispersion, zero pulse-front tilt, zero spatial chirp, and unity magnification. The device can easily be built so that its output beam remains collinear with the input beam, and when the input beam or pulse compressor moves, the input and output beams remain collinear.

Hong Li et al. [74]. He discussed the glass as an engineered material in its traditional role to control the propagation of and to spectrally modify light in the performance of optical functions. Next, he consider fluorescence, which provides the capability to convert absorbed light of a particular frequency to emitted light of a lower frequency and as a necessary condition for light amplification through spontaneous emission of radiation. Finally, he considers glass in the framework of high-energy particle physics experiments, including its use as a scintillator material and as a Cerenkov radiation detector.

Shaw et al. [75]. He invited a new chemical composition for Neodymium doped borate glass exhibiting fluorescence at 1.06 micrometers, the fluorescence from trivalent neodymium ions at a wavelength of approximately 1.06 micrometers. The glass consists essentially of about 98 weight percent of a host glass and about 2 weight percent of Nd2O3 which contributes trivalent neodymium ions to the glass. The host glass consists essentially of 20 to 80 mol percent of B2O3 and 20 to 80 mol percent of a glass modifier selected from the group consisting of Bi2 O3 and a combination of ZnO and P2O5.

Kuhn et al. [76]. He invited a method and apparatus for pumping lasant slabs, the optical pumping lamps extend transversely to the mean direction of the laser beam with the spatial period of the lamps being harmonically related to the spatial period of the zig-zag laser beam path within the slab, preferably with equal periods. In addition, the lamps are preferably positioned in registration over the lines of intersection of the central ray of the laser beam with respective broad face of the laser slab. A planar flashlamp reflector is employed for economy of fabrication. Directional lamp reflectors are employed for increasing laser efficiency and performance by discriminating against amplified surface waves.

Brown et al. [77]. He invited a slab laser apparatus having a stable/unstable resonator. The slab laser comprises a slab-shaped medium for producing a beam of coherent light. The slab-shaped medium is physically defined by an entrance end face; a rear, exiting end face; and two oppositely disposed and substantially parallel side faces. The respective end faces of the medium are disposed along an axis defining a "p" plane; the side faces are disposed along an axis defining an plane. A light beam entering at the entrance end face of the slab-shaped medium along the "p" plane axis reflects back and forth within the slab-shaped medium via total internal reflection, exiting at the rear end face. A stable optical cavity is defined for the "p" plane, comprising a hemispherical, high reflector curvature having an finite radius of curvature, and a flat, partially reflecting, outcoupler. An unstable optical resonator is defined for the plane, which operates in a low order transverse mode. The resonator in the plane consists of a high reflector mirror, and a negative radius of curvature, partially reflective mirror. The partially-reflecting outcoupler is a substantially cylindrical optical component onto which has been coated a variable reflectivity mirror (VRM) profile. The transmission of this mirror surface varies in the transverse direction. The optical component is flat in the "p" plane and cylindrical in the "s" plane. The VRM coating is disposed on the cylindrical face. The outside surface may be coated with an anti-reflective coating.

Fukae et al. [78]. He invited a specific holding structure of a slab geometry crystal for a total internal reflection, slab geometry laser (otherwise known as face pumped laser) device. Both sides of the crystal are held by side rails, and on both longitudinal end portions of the crystal o-ring backing flanges and box-shaped end pieces, respectively, are put on. Furthermore, an o-ring is put in between the end piece and the o-ring backing flange on each end portion of the crystal, and it is compressed to seal the crystal. This o-ring can be made of translucent elastomer. Accordingly, the slab geometry laser device that is compact and easy to remove from, or place into the pump station is provided.

M.S. Gaafar et al. [79]. He studied and investigated the longitudinal and shear ultrasonic wave velocities in binary Li2O-2B2O3 glasses doped with different transition metal oxides (TMOs) (where TMO = V2O5, Fe2O3, Cr2O3, NiO, TiO2, MnO2 and CuO) using pulse echo technique. Measurements were carried out at 4 MHz frequency and at room temperature. Elastic moduli and some other physical parameters such as acoustic impedance, Debye temperature, thermal expansion coefficient, and latent heat of melting were calculated. Results indicated that these parameters depend upon the TMO modifier i.e., the ionic radius of the transition metal cation.

V.P. Yanovsky et al. [80]. He developed a single frequency high power Nd:Glass laser, with a single longitudinal mode operation of the oscillator by injection seeding it with CW laser radiation. A four pass amplifier with spatial filter provided output energy of 2.7J with more than 30% extraction efficiency.

Todd S. Rutherford et al. [81]. He presents a novel design for a quasi-three-level laser. The design uses a slab laser configuration with the pump light incident from the slab edge. This allows a lower threshold and better power scaling than a conventional face-pumped slab.

F. D. Patel et al. [82, 83]. He studied electric field assisted Ag ion exchange in Nd and Yb-doped phosphate glasses to understand the role of diffusion temperature, time, and electric field during waveguide fabrication. Understanding the fabrication process allows one to produce waveguides of prescribed parameters determined for optimal Iasing characteristics. The high index changes result in large numerical apertures (NA), which are preferable for diode pumping schemes. Lasing can be theoretically achieved with the current losses in our waveguides, but lower losses, typically on the order of 0.1dB/cm, are preferable. We are currently building a diode pumped Yb:phosphate glass waveguide laser with both planar and channel guiding regions.

M.warania et al. [84]. He studied the availability of integrated optical sources in glass is expected greatly to enhance optical signal processing in glass substrates. In this paper, he report on a study of potassium ion-exchanged waveguide lasers in neodymium-doped BK-7 glass substrates. Design parameters for low-threshold waveguide lasers with high slope efficiencies are described, and methods are given for the fabrication of substrates, waveguides and laser cavities.

Campbell, J.H et al. [85]. He studied the Beamlet laser is a large aperture, flashlamp pumped Nd: glass laser that is a scientific prototype of an advanced Inertial Fusion laser. Beamlet has achieved third harmonic, conversion efficiency of near 80% with its nominal 35cm{times} 35cm square beam at mean 3{omega} fluences in excess of 8 J/cm{sup 2}(3-ns). Beamlet uses an adaptive optics system to correct for aberrations and achieve less than 2{times} diffraction limited far field spot size.

Campbell, John H. et al. [86]. He studied the advances in Nd-doped phosphate laser glasses for high-peak-power and high-average-power applications are reviewed. Compositional studies have progressed to the point that glasses can be tailored to have specific properties for specific applications. Non-radiative relaxation effects can be accurately modeled and empirical expressions have been developed to evaluate both intrinsic (structural) and extrinsic (contamination induced) relaxation effects. Losses due to surface scattering and bulk glass absorption have been carefully measured and can be accurately predicted. Improvements in processing have lead to high damage threshold (e.g. Pt inclusion free) and high thermal shock resistant glasses with improved edge claddings. High optical quality pieces up to 79 by 45 by $4cm^3$ have been made and methods for continuous melting laser glass are under development.

Izumitani et al. [87]. He invited a phosphate base laser glass comprising 55-70% P2O5, 1-15% Al2O3, 0-25% Li2 O, 0-25% Na2O, 0-8% K2 O, the total proportion of Li2 O, Na2 O, and K2 O being 10-25%, 0-15% BaO, 0-15% ZnO, 0-15% CaO, 0-15%, SrO, 0-15% MgO, the total proportion of BaO, ZnO, CaO, SrO, and MgO being 5-15%, 0-5% Y2 O3, 0-5% La2

O3, 0-5% GeO2, 0-5% CeO2, 0-3% Nb2 O5, 0-3% MnO2, 0-2% Ta2 O5, 0-1% Sb2 O3, and 0.01-5% Nd2 O3, all % being mole %. The phosphate base laser glass of this invention has a high induced emission cross section, a low non-linear refractive index coefficient, and excellent acid resistance and divitrification resistance. By replacing partially or wholely one or more of LiO2, Na2O, K2O, BaO, ZnO, CaO, SrO, MgO or Al2 O3 by LiF, NaF, KF, BaF2 ZnF2, CaF2, SrF2, MgF2 or AlF3, respectively, the above properties of the laser glass are further improved.

Bruesselbach et al. [88]. He invited a laser system having top and bottom heat-sinking bars forming the structure of the laser system and plurality of disks comprising a laser material mounted on both the bottom heat-sinking bar and the top heat-sinking bar. Also mounted on both heat-sinking bars is a plurality of pump diode bars. Each pump diode bar is preferably mounted opposite a corresponding laser disk on the opposite heat-sinking bar. The pump diode bars and the disks are symmetrically mounted on the top and bottom heat-sinking bars, so that each heat-sinking bar has an alternating pattern of pump diode bars and laser disks. The laser system is configured such that the lasing beams impinge on the disks with an incidence angle far off normal.

Beall et al. [89]. He invited a preparation of glasses exhibiting a transition temperature below 450° C., a working temperature below 500° C., and excellent resistance to attack by water and mild aqueous alkaline solutions. The glasses consist essentially, in mole percent, of at least 65% total of 23-55% ZnO, 28-40% P2O5, and 10-35% R2O, wherein R2O consists of at least two alkali metal oxides in the indicated proportions selected from the group consisting of 0-25% Li2O, 0-25% Na2O, and 0-25% K2O, and up to 35% total of optional ingredients in the indicated proportions selected from the group consisting of 0-6% Al2 O3, 0-8% B2 O3, 0-8% Al2 O3 +B2 O3, 0-15% Cu2 O, 0-5% F, 0-35% PbO, 0-35% SnO, 0-35% PbO+SnO, 0-5% ZrO2, 0-4% SiO2, and 0-15% MgO+CaO+SrO+BaO+MnO, consisting of 0-10% MgO, 0-10% CaO, 0-10% SrO, 0-12% BaO, and 0- 10% MnO.

N. M. Bobkova et al. [90]. He studied the IR spectra of glasses of the ZnO–SrO–B2O3 system with constant additions of PbO, Al2O3, and Li2O (20mol. % in sum). He established that on replacement of B2O3 by ZnO, the structure of the glasses is characterized by the presence of groupings with the bridge bonds B^{III}–O–B^{III}, B^{III}–O–B^{IV}, B^{IV}–O–B^{IV} and end groups B^{III}–O^{-}; ZnO practically exerts no influence on the coordination transition [BO3] →[BO4]. At a high content of ZnO, zinc ions are present in both a six- and a four-coordinated state.

Adolfo Speghini et al. [91]. He studied the zinc borate glasses systems of composition 4PbO.2ZnO.5B2O3 and 2PbO.4ZnO.5B2O3 doped with Pr3+, Nd3+, Eu3+, Dy3+, Ho3+ and Er3+. He investigated the absorption and luminescence spectra were measured and the Judd–Ofelt parameters. The spectroscopic behavior appears to be strongly influenced by the presence of the highly polarizable Pb2+ ion. The values of stimulated emission cross sections for selected laser transition appear to be relatively high, suggesting that these materials can be considered as interesting candidates for optical applications.

M. Bettinelli et al. [92]. He investigated a composition with 4ZnO- 3B203 glasses undoped and doped with 0.5-2.5% Eu3+ by using absorption, emission and excitation spectroscopies, fluorescence line narrowing, Raman scattering and lifetime measurements. The vibrational spectra of the undoped and doped glasses are very similar and indicate the presence of borate groups already observed in binary metaborate glasses. The Judd-Ofelt parameters and the asymmetry ratio derived from the f-f transitions of the Eu 3+ ion give information on the average local structure around the impurity ions. Crystal-field parameters obtained from site selective emission spectra are close to those found for various silicate glasses, and their major ratios are close to predictions of the Brecher and Riseberg model. A very strong phonon sideband is coupled to the 5D0 ← 7F0 transition; a value of 0.11 is obtained for the electron-phonon coupling strength.

M. Venkata et al. [93]. He studied the sound velocity and the elastic properties ofNa2O–B2O3–V2O5 glasses over a wide range of composition. Sound velocities (transverse and longitudinal) have been measured using a pulse echo superposition method at a frequency of 10 MHz. The elastic moduli (L, G, K and E), Poisson’s ratio (σ) and Debye temperature (θ) exhibit composition dependent trends. The variation of these parameters has been explained using a structural motifs present and the dimensionality of the glass network.

Yasser B. Saddeek et al. [94]. He studied glasses in the system of Na2−2xB4−4xPbxO7−6x, 0≤x≤0.8, he investigated the elastic properties and Debye temperature by using sound velocity measurements at 4 MHz. The ultrasonic parameters along with the IR spectroscopic studies have been employed to study the role of PbO on the structure of Na2B4O7 glass. The density, the molar volume, and the ultrasonic parameters of these samples have been found to be compositional dependent. The results indicate that PbO acts as a network modifier in the range 0≤x≤0.4, while beyound x = 0.4, PbO acts as a network former which affects the diborate units that mainly consist the strong borate network. These results are interpreted in terms of the IR analysis that indicates the transformation of the structural units BO3 into BO4, the increase in the number of non-bridging oxygen atoms, and the substitution of longer PbO bond length, in place of shorter BO bond. The observed compositional dependence of the elastic moduli is interpreted in terms of the effect of PbO on the boron-coordination number of the glass structure and to the relatively large electron–phonon anharmonic interactions. A good correlation was observed between the experimentally determined elastic moduli and those computed according to Makishima–Mackenzie model.

Giovanni Carini et al. [95]. He studied the acoustic properties of borate glasses by investigation of the attenuation and velocity of ultrasonic waves of frequencies in the range from 10MHz to 50MHz have been measured in (M2O)0.14(B2O3)0.86 borate glasses (M = Li, Cs or Ag) as a function of temperature between 15K and 300K. Broad relaxation peaks characterize the acoustic attenuation at temperatures below 100K and are paralleled by corresponding dispersive behaviors of the sound velocity. The velocity of sound waves decreases with increasing temperature in all the glasses, the decrease as the temperature is increased being larger in glasses containing cesium than in those with lithium or silver. Above 100K the ultrasonic velocity is regulated by the vibrational anharmonicity and shows nearly linear temperature dependence, whose slope scales with the size of the network modifier ion. The results suggest that the local motion of structural defects and the anharmonicity in borate glasses are strongly affected by the polarizing power of network modifier ions.

El Sayed Yousef et al. [96]. He studied a bismuth–borate glass doped with some rare earth ions with respect to the density, molar volume and the elastic moduli, Poisson’s ratio, Debye temperature, microhardness, softening temperature, acoustic impedance, diffusion constant and latent heat of melting. Ultrasonic velocities were measured by the pulse echo overlap technique at a frequency of 10 MHz and at room temperature. The correlation of elastic stiffness, the cross link density, and the fractal bond connectivity of these glasses are discussed. The derived experimental values of shear modulus, bulk modulus, Young’s modulus, and Poisson’s ratio for our glasses are compared with the theoretically calculated values in terms of the bond compression model and Makishima–Mackenize theory.

M.S. Gaafar et al. [97]. He studied a glass system with (1−x) [29Na2O− 4Al2O3−67B2O3]−xZnO (0≤x≤35 mol%), Elastic properties, X-ray and FT-IR spectroscopic studies have been employed to study the role of ZnO on the structure of the investigated glass system. Elastic properties and Debye temperature have been investigated using sound wave velocity measurements at 4MHz at room temperature. The results showed that the density increases and the molar volume decreases while both sound velocities and the determined glass transition temperatures decrease with increase in x. Infrared spectra of the glasses reveal that the borate network consists of diborate units and is affected by the increase in the concentration of ZnO content. These results are interpreted in terms of the decrease in the N4 values (fraction of tetrahedral coordinated boron atoms), and substitution of longer bond lengths of Zn–O in place of shorter B–O bond. The results indicate that Zinc ions have been substituted for boron ions as tetrahedral network former ions. The elastic moduli are observed to increase with the increase of ZnO content.

C. Narayana Reddy eta al. [98]. He studied a glass systems of the composition xLi2O–20ZnO–(80 _ x)B2O3 where (x = 5, 10, 15, 20, 25 and 30 mol%). Elastic properties, ^{11}B MAS-NMR and IR spectroscopic studies have been employed to study the structure of Li2O–ZnO–B2O3 glasses. Elastic properties have been investigated using sound velocity measurements at 10 MHz. Elastic moduli reveal trends in their compositional dependence. The bulk modulus and shear modulus increases monotonically with increase of BO4 units, which increase the dimensionality of the network. ^{11}B MAS-NMR and IR spectra show characteristic features of borate network and compositional dependent trends as a function of Li2O/ZnO concentration. The results are discussed in view of borate network and the dual structural role of Zn2+ ions. The results indicate that the Zn2+ is likely to occupy network forming positions in this glass system.

Giorgio Pozza et al. [99]. He investigated a system with 4ZnO. 3B203 glasses doped with Nd3+ and Er 3+ with emission transition probabilities, radiative lifetimes and fluorescence branching ratios for several excited states of theNd3+ and Er3+ ions were estimated from the room temperature absorption spectra. The stimulated emission cross sections σp for the near infrared laser transitions of Nd3+ and Er3+ were obtained from laser-excited luminescence spectra The values of that comparable to work in laser applications.

V.C. Veeranna Gowda et al. [100]. He studied the elastic properties, ^{11}B MAS–NMR and IR spectroscopic that employed to study the structure of Na2O–ZnO–B2O3 glasses. Sound velocities and elastic moduli such as longitudinal, Young’s, bulk and shear modulus have been measured at a frequency of 10 MHz as a function of ZnO concentration. Both sound velocities and elastic moduli increase with increasing ZnO concentration. Poisson’s ratio and Debye temperature were also found to increase with ZnO concentration. ^{11}B MAS–NMR and IR spectra show characteristic features of borate network and compositional dependence trends as a function of Na2O/ZnO concentration. The results are discussed in view of borate network and dual structural role of Zn2+ ion into the network. The results indicate that the Zn2+ ions are likely to occupy network forming positions in this glass system.

N.A. Abd El-Malak et al. [101]. He studied the effect of irradiation on the glass system, He used ultrasonic velocity and attenuation coefficient measured at the frequency 4MHz and at room temperature using the pulse echo technique. The effect of irradiation (1–10 Gy) on the ultrasonic attenuation, and the internal friction of the elastic properties inside the modified sodium borate glasses affected by the modification oxides CaO, ZnO, MgO, BaO, and CdO. The results indicate the possibility for using modified sodium borate glasses as γ-ray dosimeters in the low irradiation doses.

R. El-Mallawany et al. [102]. He studied a tellurite glasses in the form (TeO2)50–(V2O5)50−x(TiO2)x. Both longitudinal and shear ultrasonic velocities were measured in different compositions of the glass system by using the pulse-echo method at 5MHz frequency and at room temperature. The elastic properties of ternary telluirte glasses (TeO2)50–(V2O5)50−x(TiO2)x were measured as a function of composition. The ultrasonic velocity data, the density, the calculated elastic moduli, micro-hardness, softening temperature, and Debye temperature depend on the glass composition. He calculated the number of network bonds per unit volume, the average stretching force constant, and the average ring size, information about the structure of the glass can be deduced.

Richard.J et al. [103]. He studied the static and dynamic Vickers indentations were performed on brittle materials to investigate the rate effects in hardness, induced crack morphologies, and fracture toughness. The dynamic indentations were performed on a hardness tester, which utilizes elastic stress wave propagation phenomena in a slender rod that can deliver indentation loads of 100 ms durations. Under dynamic indentations, an increase in hardness was observed in all the brittle materials compared to their static hardness measurements. Analysis of the evolved crack morphology revealed an increase in fracture toughness for zirconia ceramics and a decrease in fracture toughness for pyrex glass under dynamic indentations.

V. Rajendran et al. [104-105]. He studied bioactive glasses of the system SiO2–Na2O–CaO–P2O5 have been prepared by the normal melting and annealing technique. The elastic moduli, attenuation, Vickers hardness, fracture toughness and fracture surface energy have been obtained using the known method at room temperature. The temperature dependence of elastic moduli and attenuation measurements has been extended over a wide range of temperature from 150 to 500 K. The SiO2 content dependence of velocities, attenuation, elastic moduli, and other parameters show an interesting observation at 45wt% of SiO2 by exhibiting an anomalous behavior. He developed a linear relation for Tg; which explores the influence of Na2O on SiO2–Na2O–CaO–P2O5 bioactive glasses. The measured hardness, fracture toughness and fracture surface energy show a linear relation with Young's modulus. It is also interesting to note that the observed results are functions of polymerisation and the number of non-bridging oxygens (NBO) prevailing in the network with change in SiO2 content. The temperature dependence of velocities, attenuation and elastic moduli shows the existence of softening in the glass network structure as temperature increases.

Appendix

Glass Laser Transitions

Table1.4 Glass Laser Transitions [48]

Wavelength* (μm)	Ion	Transition
0.38	Nd3+	4D3/2 → 4I11/2
0.41	Nd3+	2P3/2 → 4I11/2
0.46	Tm3+	1D2 → 3F4
0.48	Tm3+	1G4 → 3H6
0.49	Pr3+	3P0 → 3H4
0.52	Pr3+	3P1 → 3H5
0.54	Tb3+	5D4 → 7F5
0.55	Er3+	4S3/2 → 4I15/2
0.55	Ho3+	5S2 → 5I8
0.61	Pr3+	3P0 → 3H6
0.64	Pr3+	3P0 → 3F2
0.65	Sm3+	4G5/2 → 6H9/2
0.70	Pr3+	3P1 → 3F4
0.72	Pr3+	3P1 → 3F4
0.75	Ho3+	5S2 → 5I7
0.82	Tm3+	3H4 → 3H6
0.85	Er3+	4S3/2 → 4I13/2

0.88	Pr3+	3P1 → 1G4
0.89	Pr3+	3P0 → 1G4
0.93	Nd3+	4F3/2 → 4I9/2
0.93	Pm3+	5F1 → 5I5
0.99	Er3+	4I11/2 → 4I15/2
1.03	Yb3+	2F5/2 → 2F7/2
1.06	Nd3+	4F3/2 → 4I11/2
1.08	Pr3+	1D2 → 3F3,4
1.10	Pm3+	5F1 → 5I6
1.2	Ho3+	5I6 → 5I8
1.31	Pr3+	1G4 → 3H5
1.34	Nd3+	4F3/2 → 4I13/2
1.38	Ho3+	5S2,5F4 → 5I5
1.48	Tm3+	3H4 → 3F4
1.51	Tm3+	1D2 → 1G4
1.55	Er3+	4I13/2 → 4I15/2
1.66	Er3+	2H11/2 → 4I9/2
1.72	Er3+	4S3/2 → 4I9/2
1.88	Tm3+	3F4 → 3H6
2.05	Ho3+	5I7 → 5I8
2.3	Tm3+	3H4 → 3H5
2.75	Er3+	4I11/2 → 4I13/2
2.9	Ho3+	5I6 → 5I7
3.5	Er3+	4F9/2 → 4I9/2
3.9	Ho3+	5I5 → 5I6

*Wavelengths of transitions are only approximate; exact wavelengths are dependent on the host and temperature and the specific Stark levels involved.

Table1.5 Ions in Glasses Exhibiting Gain [48]

Wavelength (μm)	Ion	Host glass (sensitizer)	Form
0.543	Ho3+	fluorozircoaluminate (Yb)	fiber
0.546	Er3+	Fluorozirconate	fiber
0.560–0.585	Cu+	aluminoborosilicate	bulk
0.625	CdSSe	Silicate	bulk
0.633	Cu+	Fluorohafnate	bulk
1.083	Nd3+	Chalcogenide	fiber
1.536	Er3+	Silica	fiber
2.05	Ho3+	alumino-zircofluoride(Tm3+)	bulk

Table1.6 Glass Lasers Arranged in Order of Increasing Wavelength [48]

Wavelength(a) (μm)	Ion	Host glass (b)	Form
0.381	Nd3+	Fluorozirconate	Fiber
0.412	Nd3+	Fluorozirconate	Fiber
0.455	Tm3+	Fluorozirconate	Fiber
0.480	Tm3+	Fluorozirconate	Fiber
0.482	Tm3+	Fluorozirconate	Fiber
0.491	Pr3+	Fluorozirconate	Fiber
0.491–0.493	Pr3+	fluorozirconate (Yb)	Fiber
0.492	Pr3+	Fluorozirconate	Fiber
0.517–0.540	Pr3+	fluorozirconate (Yb)	Fiber
0.520	Pr3+	Fluorozirconate	Fiber
0.521	Pr3+	Fluorozirconate	Fiber
~0.539–550	Ho3+	Fluorozirconate	Fiber
0.54(c)	Tb3+	Borate	Bulk
0.540–0.545(d)	Er3+	Fluorozirconate	Fiber
0.540–0.553	Ho3+	Fluorozirconate	Fiber
0.546	Er3+	Fluorozirconate	Fiber
0.548	Er3+	fluorozirconate	Fiber
0.599–0.611	Pr3+	fluorozirconate	Fiber
0.601–0.618	Pr3+	fluorozirconate	Fiber
0.602	Pr3+	fluorozirconate (Yb)	Fiber
0.605	Pr3+	fluorozirconate	Fiber
0.605–0.622	Pr3+	fluorozirconate (Yb)	Fiber
0.631–0.641	Pr3+	fluorozirconate	Fiber
0.6328	Pr3+	fluorozirconate	Fiber
0.635	Pr3+	fluorozirconate	Fiber
0.635	Pr3+	fluorozirconate (Yb)	Fiber
0.635–0.637	Pr3+	fluorozirconate (Yb)	Fiber
0.651	Sm3+	silica	Fiber
0.690–0.703	Pr3+	fluorzirconate	Fiber
0.707–0.725	Pr3+	fluorozirconate	Fiber
0.715	Pr3+	fluorzirconate	Fiber
0.7495–0.7545	Ho3+	fluorozirconate	Fiber

0.800–0.830	Tm3+	fluorozirconate	Fiber
0.803–0.816	Tm3+	fluorozirconate	Fiber
0.815–0.825	Tm3+	fluorozirconate	Fiber
0.85	Er3+	fluorozirconate	Fiber
0.880–0.886	Pr3+	fluorozirconate	Fiber
0.89	Pr3+	silica (Ge)	Fiber
0.899–0.951	Nd3+	silica	Fiber
0.902–0.916	Pr3+	fluorozirconate	Fiber
0.905	Nd3+	phosphate	Planar
0.918	Nd3+	Na–Ca silicate	Bulk
0.92	Nd3+	silicate	Bulk
0.933	Pm3+	Pb–In phosphate	Bulk
0.938	Nd3+	silica	Fiber
0.974	Yb3+	silica	Fiber
0.980	Yb3+	silica (Al,P)	Fiber
0.981–1.004	Er3+	fluorozirconate	Fiber
1.00	Er3+	fluorozirconate	Fiber
1.000–1.050	Yb3+	fluorozirconate	Fiber
1.000–1.085	Pr3+	silica	Fiber
1.010– 1.162	Yb3+	silica	Fiber
1.015	Yb3+	Li–Mg–Al silicate	Bulk
1.015–1.140	Yb3+	silica	Fiber
1.018	Yb3+	Ca–Li borate (Nd)	Bulk
1.020	Yb3+	fluorozirconate	Fiber
1.028–1.064	Yb3+	silica	Fiber
1.047	Nd3+	fluoroberyllate	Bulk
1.05	Nd3+	phosphate	Fiber
1.05	Nd3+	phosphate (LG–760)	Planar
1.050	Nd3+	fluorozirconate	Fiber
1.050–1.075	Nd3+	silicate (P)	Fiber
1.051	Nd3+	fluorophosphate	Bulk
1.051	Nd3+	fluorozirconate	Microsphere
1.0515	Nd3+	silica (P)	Planar
1.0525	Nd3+	silica (P)	Planar
1.053	Nd3+	silica	Planar
1.0535	Nd3+	Na–K–Cd phosphate	Bulk
1.054	Nd3+	phosphate (LHG–5)	Planar
1.054	Nd3+	phosphate (LHG–8)	Bulk
1.054	Nd3+	Zn–Li phosphate	Bulk
1.0546	Nd3+	phosphate (APG-1)	Bulk
1.055	Nd3+	Li–Nd–La phosphate	Bulk
1.055	Nd3+	silica (P)	Fiber
1.057	Nd3+	silicate (LG–660)	Planar
1.057	Nd3+	phosphate	Planar
1.058	Nd3+	borosilicate (BK–7)	Planar
1.06	Nd3+	Ba silicate	Planar
1.06	Nd3+	borate	Bulk
1.06	Nd3+	borosilicate	Planar

1.06	Nd3+	glass ceramic	Bulk
1.06	Nd3+	lead silicate (F7)	Fiber
1.06	Nd3+	Li germanate	Bulk
1.06	Nd3+	Li–La phosphate (Cr)	Bulk
1.06	Nd3+	silicate	Bulk
1.06	Nd3+	silicate	Fiber
~1.06	Nd3+	silicate (GLS2,GLS3)	Planar
1.06	Yb3+	K–Ba silicate	Bulk
1.060	Nd3+	silica (Al)	Fiber
1.060	Nd3+	silica (Al)	Planar
1.0605	Nd3+	Li tellurite	Bulk
1.061	Nd3+	K–Ba silicate	Bulk
1.061	Nd3+	tellurite	Fiber
1.062	Nd3+	silicate (buffer)	Bulk
1.0635	Nd3+	silica (Al)	Bulk
1.064	Nd3+	Ba silicate	Planar
1.066	Nd3+	tellurite	Bulk
1.069–1.144	Nd3+	silica	Fiber
1.08	Nd3+	chalcogenide (Ga:La:S)	Bulk
1.08	Pr3+	silica	Bulk
1.088	Nd3+	silica (Al)	Fiber
1.088	Nd3+	silica (Ge)	Fiber
1.098	Pm3+	Pb–In phosphate	Bulk
1.12	Yb3+	silica (Ge)	Fiber
1.128	Yb3+	germanosilicate	Fiber
1.134	Yb3+	germanosilicate	Fiber
1.19	Ho3+	fluorozirconate	Fiber
1.24–1.34	Pr3+	fluorozirconate	Fiber
1.28–1.34	Pr3+	fluorozirconate	Fiber
1.290–1.320	Pr3+	fluorozirconate	Fiber
1.294	Pr3+	fluorozirconate	Fiber
1.3	Pr3+	fluorozirconate (Yb)	Fiber
1.31	Pr3+	fluorozirconate	Fiber
1.310–1.370	Nd3+	fluorozirconate	Fiber
1.31–1.36	Nd3+	fluorozirconate	Fiber
1.32	Nd3+	Li–Nd–La phosphate	Bulk
1.323	Nd3+	fluorophosphate	Fiber
1.325	Nd3+	phosphate (LHG–5)	Planar
1.328	Nd3+	fluorophosphate	Fiber
1.334	Nd3+	fluorozirconate	Microsphere
1.338	Nd3+	fluorozirconate	Fiber
1.340	Nd3+	fluorozirconate	Fibers
1.345	Nd3+	fluorozirconate	Fiber
1.350	Nd3+	fluorozirconate	Fiber
1.355	Nd3+	fluorophosphate	Fiber
1.355	Nd3+	phosphate (LHG–5)	Planar
1.356	Nd3+	phosphate	Planar
1.36	Nd3+	silica (P)	Fiber

1.363	Nd3+	phosphate	Fiber
1.366	Nd3+	phosphate (LHG–8)	Fiber
1.37	Nd3+	La–Ba–Th borate	Bulk
1.38	Ho3+	fluorozirconate	Fiber
1.46–1.51	Tm3+	fluorozirconate	Fiber
~1.47	Tm3+	fluorozirconate	Fiber
1.47	Tm3+	Fluorozirconate (Tb3+)	Bulk
1.475	Tm3+	fluorozirconate	Fiber
1.475(e)	Tm3+	fluorozirconate	Fiber
1.48	Tm3+	fluorozirconate	Fiber
1.481	Tm3+	fluorozirconate (Tb)	Fiber
1.50–1.70	Er3+	silica	Fiber
1.51	Tm3+	fluorozirconate	Fiber
1.52–1.57	Er3+	silica (Ge,Al,P)	Fiber
1.527–1560	Er3+	aluminosilicate	Fiber
1.529–1.554	Er3+	silica	Fiber

(a) If a tuning range is reported, the laser is listed by the lowest wavelength cited.
(b) Codopant and fluorescence sensitizing ions are included in parentheses.
(c) Proof of lasing was based on the appearance of emission spikes.
(d) Co-lasing at 1.55 μm.
(e) Co-lasing at 1.88 μm.

References

1. D.A. Rayan, Y.H. Elbashar, A.B. El Basaty and M.M. Rashad, “Infrared spectroscopy of cupric oxide doped barium phosphate glass”, Research Journal of Pharmaceutical, Biological and Chemical Sciences (RJPBCS), volume 6, issue 3, May – June 2015, pages 1026-1030
2. Yahia H.Elbashar, "Structural and spectroscopic analyses of copper doped P2O5-ZnO- K2O-Bi2O3 glasses", International Journal: Processing and application of ceramics, 9 [3] (2015) 169–173
3. Y.H.Elbashar, Aly Saeed, “Computational spectroscopic analysis by using Clausius–Mossotti method for sodium borate glass doped neodymium oxide”, Research Journal of Pharmaceutical, Biological and Chemical Sciences (RJPBCS), volume 6, issue 5, September – October 2015, Pages 320-326
4. Aly Saeed, Y. H. Elbashar, S. U. El Kameesy, “Study of Gamma Ray Attenuation of High-Density Bismuth Silicate Glass for shielding applications”, Research Journal of Pharmaceutical, Biological and Chemical Sciences (RJPBCS), volume 6, issue 4, July – August 2015, pages 1830-1837
5. Aly Saeed, Y. H. Elbashar, S. U. El Kameesy, “Towards modeling of copper-phosphate glass for optical bandpass absorption filter” , Research Journal of Pharmaceutical, Biological and Chemical Sciences (RJPBCS), volume 6, issue 4, July – August 2015 , pages 1390- 1397
6. Y. H. Elbashar, Aly Saeed, D.A. Rayan ,“ Prism method of studying the refractive index for zinc borate sodium glass doped neodymium oxide”, Journal of Ceramic Processing Research(JCPR), Vol. 17, No. 6, pp. 532-536 (2016)

7. Y. H. Elbashar, Aly Saeed and S. S. Moslem, "Spectroscopic Analysis of Copper Calcium Phosphate Glasses Matrix", Nonlinear Optics and Quantum Optics (NLOQO), (2016) Volume 48, Number 1, p. 41-48
8. Y.H.Elbashar, D.A. Rayan, "Judd Ofelt study of absorption spectrum for neodymium doped borate glass", International Journal of Applied Chemistry (IJAC) , Volume 12, Number 1 (2016) pp. 57-63
9. Y.H.Elbashar, D.A. Rayan, "Thermal analysis of B2O3-Na2O-ZnO glass doped Nd2O3", International Journal of Applied Engineering Research (IJAER), Volume 11, Number 8 (2016) pp. 5791-5796
10. Aly Saeed, Y. H. Elbashar, R. M. El shazly,"Optical Properties of High Density Barium Borate Glass for Gamma Ray Shielding Applications", Journal of Optical and Quantum Electronics (2016) 48:1
11. M.S.Abdel-Gayed, Y.H.Elbashar, M.H.Barakat, M.R.Shehata,"Optical Spectroscopic Investigations on Silver doped Sodium Phosphate Glass", Journal of Optical and Quantum Electronics, DOI 10.1007/s11082-017-1132-2, September 2017, 49:305
12. Yahia. H. Elbashar, Diaa .A. Rayan, Hossam S. Rady, "Molecular spectroscopic study of borate glass doped neodymium oxide", Nonlinear Optics and Quantum Optics NLOQO, Volume 48, Number 3 (2017),p. 237-245
13. Y.H.Elbashar, H.A. Abd El-Ghany, "Optical spectroscopic analysis of Fe2O3 doped CuO containing phosphate glass", Journal of Optical and Quantum Electronics, DOI 10.1007/s11082-017-1126-0, August 2017, 49:310
14. Aly Saeed, R. M. El shazly, Y. H. Elbashar, A. M. Abou El-azm, M. M. El-Okr, M.N.H.Comsan, A. M. Osman, A. M. Abdal-monem, A. R. El-Sersy, "Neutron shielding properties of a borated high-density glass", Journal of Nuclear Technology and Radiation Protection, 2017, Vol. 32, No. 2, pp. 120-126
15. Y.H.Elbashar, D.A. Rayan, M.M. Rashad ," Protection Glass Eyewear Against a YAG Laser Based on a Bandpass Absorption Filter ", Journal of Silicon, DOI 10.1007/s12633-015-9389-1, January 2017, Volume 9, Issue 1, pp 111–116
16. Y.H.Elbashar," Design and fabrication of protection window against YAG laser", Journal of Silicon, DOI 10.1007/s12633-016-9429-5, September 2017, Volume 9, Issue 5, pp 711–715
17. Aly Saeed, Y. H. Elbashar , S. U. El Khameesy," A Novel Barium Borate Glasses for Optical Applications", Journal of Silicon, DOI: 10.1007/s12633-016-9492-y , March 2018, Volume 10, Issue 2, pp 569–574
18. Y.H.Elbashar, A.E.Omran , J. A. Khaliel , A.S. Abdel-Rahaman,H. H. Hassan, "Ultraviolet transmitting glass matrix for low power laser lens", Nonlinear Optics and Quantum Optics, NLOQO, 2018, Vol 49.Number 3-4, p. 247-265
19. Aly Saeed, Y. H. Elbashar, S. U. El Kameesy, " Optical Spectroscopic Analysis of High Density Lead BoroSilicate Glasses", Journal of Silicon, DOI 10.1007/s12633-015-9391-7, March 2018, Volume 10, Issue 2, pp 185–189
20. Y.H. Elbashar, M.M. Rashad, D.A. Rayan, "Physical and mechanical properties of neodymium doped zinc borate glass with different boron content", Journal of Silicon, DOI 10.1007/s12633-015-9383-7, January 2018, Volume 10, Issue 1, pp 115–122
21. Y.H.Elbashar, W.A.Rashidy , J.A. Khaliel, D.I. Moubarak, A.S. Abdel-Rahaman, H. H. Hassan, "Optical Spectroscopic study of hard ultraviolet protection sunglasses", Journal of Nonlinear Optics and Quantum optics (Accepted under process)
22. Y.H.Elbashar, S.M.Hussien , J.A. Khaliel, D.I. Moubarak, A.S. Abdel-Rahaman, H. H. Hassan, "Optical spectroscopic analysis of sodium zinc phosphate glass doped cadmium oxide used for laser window protection", Annals of the University of Craiova, Physics , Physics AUC, vol. 28, 57-72 (2018)

23. Y.H.Elbashar, R.A.Ibrahem , J.A. Khaliel, D.I. Moubarak, A.S. Abdel-Rahaman, H. H. Hassan, "Optical spectroscopic analysis of bandpass absorption glass filter based on vanadium copper oxide for laser safety applications", Journal of Nonlinear Optics and Quantum optics(Accepted under process)
24. Yahia.H.Elbashar, S. S. Moslem, Diaa.A. Rayan, Hussam. H. Hassan, "The influence of nickel ions on the electric behavior of P_2O_5–ZnO–Na_2O glassy system", Journal of Microwave Power and Electromagnetic Energy (Accepted under process)
25. Y. S. Nada, J. M. El-Azab, S. M. Maize, Y.H.Elbashar, "Pulsed Solid-State Laser Systems Using ABCD Matrix Method: A Review", Journal of Nonlinear Optics and Quantum optics (Accepted under process)
26. Y. H. Elbashar, D. A. Rayan , H. S. Ayoub , M.S. Abdel-Gayed , S.M.Hussien , A.E.Omran, W.A.Rashidy , R.A.Ibrahem , M.A. Mohamed, D.I. Moubarak , Mohamed Ahmed Eassa , Khaled Hussein Metwaly , "Electric, Dielectric and Optical Properties of Doped Metal Oxide Glasses: A Review", Journal of Nonlinear Optics and Quantum optics (Accepted under process)
27. Esmat M. Elfeky, Yahia H. Elbashar, Mohammad H. Barakat, Mohamed R. Shehata, Safaa S. Hassan, "Structural investigation and applications of glassy sodium phosphate including the kinetics of dissolution rates and spectral analysis of the prepared samples with a focus on their effects on water treatment", Optical and quantum electronics , doi.org/10.1007/s11082-019-1822-z, (2019) 51:102
28. D. A. Rayan, Y.H.Elbashar , M.M. Rashad , and A. El-Korashy, " Optical Spectroscopic analysis of phosphate barium glass doped cupric oxide for bandpass absorption filter ", Journal of Non- crystalline solids, Volume 382, 15 December 2013, Pages 52–56
29. Aly Saeed, R. M. El shazly, Y. H. Elbashar, A. M. Abou El-azm, M. M. El-Okr, M.N.H.Comsan, A. M. Osman, A. M. Abdal-monem, A. R. El-Sersy, “Gamma Ray Attenuation in Developed Borate Glassy”, Journal of Radiation Physics and Chemistry, Volume 102, September 2014, Pages 167-170
30. Nehal Aboulfotoh, Yahia Elbashar, Mohamed Ibrahem, Mohamed Elokr, "Characterization of copper doped phosphate glasses for optical applications", Journal of Ceramics International ,Volume 40, Issue 7, Part B, August 2014, Pages 10395–10399

31. James E. Shelby, Introduction to Glass Science and Technology, Second Edition, the Royal Society of Chemistry 2005
32. Robert H. Doremus, Glass Science, Second Edition, John Wiley & Sons, Inc., 1994
33. K. J. Rao, Structural Chemistry of Glasses, Elsevier Science & Technology Books, 2002
34. C. Suryanarayana and A. Inoue, Bulk Metallic Glasses, Taylor and Francis Group, LLC, 2011
35. Donald E. Garrett, Borates: handbook of deposits, processing, properties, and use, Academic Press; 1st edition, 1998
36. John Mauro, Glass Properties and Their Relationships to Network Forming and Modifying Agents, New York State College of Ceramics at Alfred University,2000
37. W. H. Zachariasen, J. Am. Chem. Soc., 54, 3841 (1932)
38. W. Vogel, Chemistry of Glass, Columbus: The American Ceramic Society, 1985.
39. K. Varshneya, Fundamentals of Inorganic Glasses, San Diego Academic Press, Inc., 1994
40. P. J. Bray, Interaction of Radiation with Solids, New York: Plenum Press, 1967
41. Mary Elvira Weeks, Discovery of the Elements, Journal of Chemical Education, Easton, Pa., 6Th Edition, 1956
42. G. Adachi, Nobuhito Imanaka and Z.C. Kang, Binary Rare Earth Oxides, Springer, 2004
43. Guokui Liu, Bernard Jacquier, Spectroscopic Properties of Rare Earths in Optical Materials, Springer, 2005
44. P. Enghag, Encyclopedia of the Elements - Technical Data - History - Processing - Applications, WILEY-VCH Verlag GmbH & Co KGaA, 2004
45. Karl A. Gschneidner, Jr. and LeRoy Eyring, Handbook on the Physics and Chemistry of Rare Earths, Volume 3, 1979
46. K.A. Gschneidner, Jr., J.-C.G. Bünzli and V.K. Pecharsky, Handbook on the Physics and Chemistry of Rare Earths ,Vol. 37, Elsevier B.V., 2007
47. Michel J. F. Digonnet, Rare-Earth-Doped Fiber Lasers and Amplifiers Second Edition, Revised and Expanded,Marcel Dekker, Inc., 2001
48. Glass lasers, K.Patek, Butterworth & Co (Publishers) Ltd., 1970
49. Marvin J. Weber, Handbook of laser wavelengths,Boca Raton: CRC Press LLC, 1999
50. Hong Li, Mark J. Davis, and Alexander J. Marker, III,Glass and Light, International Journal of Applied Glass Science 1 [1] 63–73 (2010)
51. Funk, D. S., Carlson, J.W. and Eden, J. G., Ultraviolet (381 nm) room temperature laser in neodymium-doped fluorozirconate fibre, Electron. Lett. 30, 1859 (1994)
52. Funk, D. S., Carlson, J. W. and Eden, J. G., Room temperature fluorozirconate glass fiber laser in the violet (412 nm), Optics Lett. 20, 1474 (1995)
53. M. Nikl , J. Pejchal , R. Jinhua , J. Zhang , G. Chen ,Photoluminescence of ZnO-aggregates in oxide glasses, Optical Materials 29 (2007) 552–555
54. J.H. Campbell , T.I. Suratwala, Nd-doped phosphate glasses for high-energy/high-peak-power lasers, Journal of Non-Crystalline Solids 263&264 (2000) 318-341
55. Xiushan Zhu , N. Peyghambarian, High-Power ZBLAN Glass Fiber Lasers: Review and Prospect, Advances in OptoElectronics ISSN 1687-563X Volume: 2010; Date: 2010
56. S.P. Tandon, Y.K. Sharma, N.B. Bishnoi and K. Tandon, Optical Studies on Rare Earth Lasing Materials, Defence Science Journal, Vol 47, No 2, 1997.pp. 225-238
57. M. Weber, J. Myers, D. Blackburn, "Optical Properties of Nd3+ in Tellurite and Phosphotelurite Glasses", J. Appl. Phys. 52(4) April 1981

58. S. Jiang, J. Myers, D. Rhonehouse, M. Myers, S. Hamlin, J. Lucas, "Simultaneous Dual and Multiple Wavelength Operation and Laser Performance of 1.3 μm Transition in Various Nd3+ Doped Glasses", Photonics West, SPIE Proceedings Vol. 2698, 1996
59. H. Jiang, J. Myers, D. Rhonehouse, M. Myers, J. Ballato, "Rare-Earth-Doped Phosphate Glasses for Neodymium Laser Systems Possessing a Greatly Enhanced Pump Power Conversion", Presented at the American Ceramic Society, 102nd Annual Meeting & Exposition, St. Louis, MO, April 30-May 3, 2000
60. E. Siegman, Y. Chen, V. Sudesh, M. Richardson, M. Bass, P. Foy, W. Hawkins, J. Ballato, "Confined Propagation and Near Single-Mode Laser Oscillation in a Gain-Guided, Index Antiguided Optical Fiber", Applied Physics Letters 89, 251101, 2006
61. R. Jacobs, M. Weber, "Dependence of the 4F3/2 - 4I11/2 Induced-Emission Cross Section for Nd3+ on Glass Composition", IEEE J. of Quantum Electronics, Vol. QE012, No. 2, Feb. 1976
62. C. Jacinto, S. Oliveira, T. Catunda, A. Andrade, J. Myers, M. Myers, "Upconversion Effect on Fluorescence Quantum Efficiency and Heat Generation in Nd3+-doped Materials", Optics Express 2040, Vol. 13, No. 6, March, 21, 2005
63. C. Jacinto, S. Oliveira, L. Nunes, J. Myers, M. Myers, T. Catunda, "Normalized-Lifetime Thermal-Lens Method for the Determination of Luminescence Quantum Efficiency and Thermo-Optical Coefficients: Application to Nd3+ - Doped Glasses", Physical Review B 73, 125107, 2006
64. S. Oliveira, C. da Silva, L. Nunes, T. Catunda, J. Myers, M. Myers, "Quantum Efficiency of 4F3/2Level and Loss Mechanisms in Nd3+-doped Phosphate Laser Glass", OSA, Conference on Leasers & ElectroOptics, (CLEO) 2004
65. J. Myers, R. Wu, M. Myers, "New High Power Rare-Earth-Doped Fiber Laser Materials and Architectures", Submitted to: SPIE, International Symposium on LASE 2003, Photonics West 2003, Fiber Lasers (LA15), San Jose, CA January28-30, 2003
66. R. Wu, J.D. Myers, M.J. Myers, "Nd-Doped Cladding Pumped Fiber Laser", OSA Conference, Optics in the Southeast, Fiber Optics and Communication Technologies, Clemson University, October 4-5, 2001
67. S. Mohan, K. S. Thind, and G. Sharma,, Effect of Nd3+ Concentration on the Physical and Absorption Properties of Sodium-Lead-Borate Glasses, Brazilian Journal of Physics, vol. 37, no. 4, December, 2007, pp 1306-1313
68. S. Jiang, J. Myers, R. Wu, G. Bishop, D. Rhonehouse, M. Myers, S. Hamlin, "Chemical Strengthened Er3+, Nd3+ Doped Phosphate Laser Glasses", SPIE Vol. 2379, 1995
69. Wojciech A. Pisarski , Joanna Pisarska , Witold Ryba-Romanowski, Structural role of rare earth ions in lead borate glasses evidenced by infrared spectroscopy: BO34←→BO4 conversion ,Journal of Molecular Structure 744–747 (2005) 515–520
70. J. Furthner, A. Penzkofer, Emission spectra and cross-section spectra of neodymium laser glasses,Optical and Quantum Electronics 24 (1992) 591-601
71. M. ZAHIR, R. OLAZCUAGA, C. PARENT, G. LE FLEM and P. HAGENMULLER , A STRUCTURAL INTERPRETATION OF THE Pb 2+, Eu 3+ AND Nd 3+ OPTICAL SPECTRA IN DOPED SODIUM BORATE GLASSES,Journal of Non-Crystalline Solids 69 (1985) 221-229
72. A.E. Burns, D.W. Winslow, W.J. Clarida , M. Affatigato , S.A. Feller , R.K. Brow , Structure of binary neodymium borate glasses by infrared spectroscopy, Journal of Non-Crystalline Solids 352 (2006) 2364–2366

73. L. Del Longo, M. Ferrari, E. Zanghellini , M. Bettinelli, J.A. Capobianco, M. Montagna, F. Rossi,Optical spectroscopy of zinc borate glass activated by Pr3+‡ ions, Journal of Non-Crystalline Solids 231 (1998) 178-188
74. Selcuk Akturk, Xun Gu, Mark Kimmel, Rick Trebino, Extremely simple single-prism ultrashort-pulse compressor,16 October 2006 / Vol. 14, No. 21 / OPTICS EXPRESS, 10101-10108
75. Hong Li, Mark J. Davis, and Alexander J. Marker, Glass and Light, International Journal of Applied Glass Science 1 [1] 63–73 (2010)
76. Shaw, Robert R., Snitzer, Elias, Neodymium doped borate glass exhibiting fluorescence at 1.06 micrometers ,United States Patent 3867303, Publication Date 02/18/1975
77. Kuhn, Kelin J. , Method and apparatus for pumping lasant slabs, United States Patent 4617669 , Publication Date 10/14/1986
78. Brown, David C, Benfey, David P. , Slab laser, United States Patent 5299220 ,Publication Date 03/29/1994
79. Fukae, Kenneth , Slab geometry laser device, United States Patent 4653061, Publication Date 03/24/1987
80. M.S. Gaafar , F.H. El-Batal , M. El-Gazery and S.A. Mansour,Effect of Doping by Different Transition Metals on the Acoustical Properties of Alkali Borate Glasses, ACTA PHYSICA POLONICA A, No. 3, Vol. 115 (2009) pp 671-678
81. Yanovsky, V.P. Richardson, M.C. Miesak, E.J., Compact, single-frequency, high-power Nd: glass laser , IEEE Journal of Quantum Electronics, Vol30 Issue: 4 ,1994,pp 884 – 886
82. Todd S. Rutherford, William M. Tulloch, Eric K. Gustafson, and Robert L. Byer, Edge-Pumped Quasi-Three-Level Slab Lasers:Design and Power Scaling , IEEE JOURNAL OF QUANTUM ELECTRONICS, VOL. 36, NO. 2, FEBRUARY 2000
83. F. D. Patel, E. C. Honea, D. Krol,S. A. Payne, J. S. Hayden, Nd3+and Yb3+Doped Phosphate Glass Waveguides Fabricated Using Electric Field Assisted Ag+ Diffusion, UCRL-JC-12SS17 PREPRINT
84. F. D. Pate& E. C. Honea, D. Krol, S. A. Payne, J. S. Hayden, Waveguide Fabrication in Nd3+ and Yb3+ Doped Phosphate Glasses, UCRL-JC-128624 PREPRINT
85. Mwarania, E. K., Wang, J., Lane, J. and Wilkinson, J. S. (1993) Neodymium-doped ion-exchanged waveguide lasers in BK-7 glass. IEEE Journal of Lightwave Technology, 11 (10). pp. 1550-1558
86. Campbell, J.H. ; Barker, C.E. ; VanWonterghem, B.M. ; Speck, D.R. ; Behrendt, W.C. ; Murray, J.R. ; Caird, J.A. ; Decker, D.E. ; Smith, I.C. , Performance results for Beamlet: A large aperture multipass Nd glass laser, CLEO/Pacific Rim coal conference, Makuhar (Japan), 11-14 Jul 1995 ; PBD: 11 Apr 1995
87. Campbell, John H., Recent advances in phosphate laser glasses for high-power applications, UCRL-JC-124244
88. Izumitani, Tetsuro , Tsuru, Michitaka , Phosphate base laser glasses, United States Patent 4239645 ,Publication Date:12/16/1980
89. Bruesselbach, Hans W., Sumida, David S.,Multiple-disk laser system, United States Patent 6987789, Publication Date:01/17/2006
90. Beall, George H. , Quinn, Candace J.,Zinc-containing phosphate glasses, United States Patent 4940677, Publication Date:07/10/1990
91. N. M. Bobkova and S. A. Khot'ko, Structure of zinc-borate low-melting glasses derived from IR spectroscopy data, Journal of Applied Spectroscopy, Vol. 72, No. 6, 2005, 853-857

92. Adolfo Speghini, Massimo Peruffo, Maurizio Casarin, David Ajo`, Marco Bettinelli , Electronic spectroscopy of trivalent lanthanide ions in lead zinc borate glasses, Journal of Alloys and Compounds 300–301 (2000) 174–179
93. M. Bettinelli , A. Speghini , M. Ferrari, M. Montagna, Spectroscopic investigation of zinc borate glasses doped with trivalent europium ions,Journal of Non-Crystalline Solids 201 (1996) 211-221
94. M. Venkata ,Subba Reddy , M. Sudhakara Reddy , C. Narayana Reddy , R.P.S. Chakradhar , Elastic properties of Na2O–B2O3–V2O5 glasses, Journal of Alloys and Compounds 479 (2009) 17–21
95. Yasser B. Saddeek, Structural and acoustical studies of lead sodium borate glasses, Journal of Alloys and Compounds 467 (2009) 14–21
96. Giovanni Carini , Giuseppe Carini , Emanuele Cosio ,Giovanna DAngelo, Gaspare Tripodo, Antonio Bartolotta, Acoustic properties of borate glasses, Journal of Non-Crystalline Solids 345&346 (2004) 473–477
97. El Sayed Yousef, Amin El-Adawy, N. El-KheshKhany, Effect of rare earth (Pr2O3, Nd2O3, Sm2O3, Eu2O3, Gd2O3 and Er2O3) on the acoustic properties of glass belonging to bismuth–borate system, Solid State Communications 139 (2006) 108–113
98. M.S. Gaafar, N.S. Abd El-Aal, O.W. Gerges , G. El-Amir, Elastic properties and structural studies on some zinc-borate glasses derived from ultrasonic, FT-IR and X-ray techniques, Journal of Alloys and Compounds 475 (2009) 535–542
99. C. Narayana Reddy , R.P. Sreekanth Chakradhar, Elastic properties and spectroscopic studies of fast ion conducting Li2O–ZnO–B2O3 glass system, Materials Research Bulletin 42 (2007) 1337–1347
100. Giorgio Pozza ,David Ajo, Marco Bettinelli, Adolfo Speghini, Maurizio Casarin , ABSORPTION AND LUMINESCENCE SPECTROSCOPY OF Nd 3+ AND Er 3+ IN A ZINC BORATE GLASS, Solid State Communications, Vol. 97, No. 6, pp. 521 525, 1996
101. V.C.VEERANNA GOWDA and R.V.ANAVEKAR , Elastic properties and spectroscopic studies of Na2O–ZnO–B2O3 glass system, Bull. Mater. Sci., Vol. 27, No. 2, April 2004, pp. 199–205
102. N.A. Abd El-Malak, Ultrasonic studies on irradiated sodium borate glasses, Materials Chemistry and Physics 73 (2002) 156–161
103. R. El-Mallawany, N. El-Khoshkhany, H. Afifi, Ultrasonic studies of (TeO2)50–(V2O5)50−x(TiO2)x glasses, Materials Chemistry and Physics 95 (2006) 321–327
104. Richard J. Anton, Ghatu Subhash, Dynamic Vickers indentation of brittle materials, Wear 239 2000. 27–35
105. V. Rajendran, A. Nishara Begum, M.A. Azooz, F.H. El Batal , Microstructural dependence on relevant physical–mechanical properties on SiO2–Na2O–CaO–P2O5 biological glasses, Biomaterials 23 (2002) 4263–4275